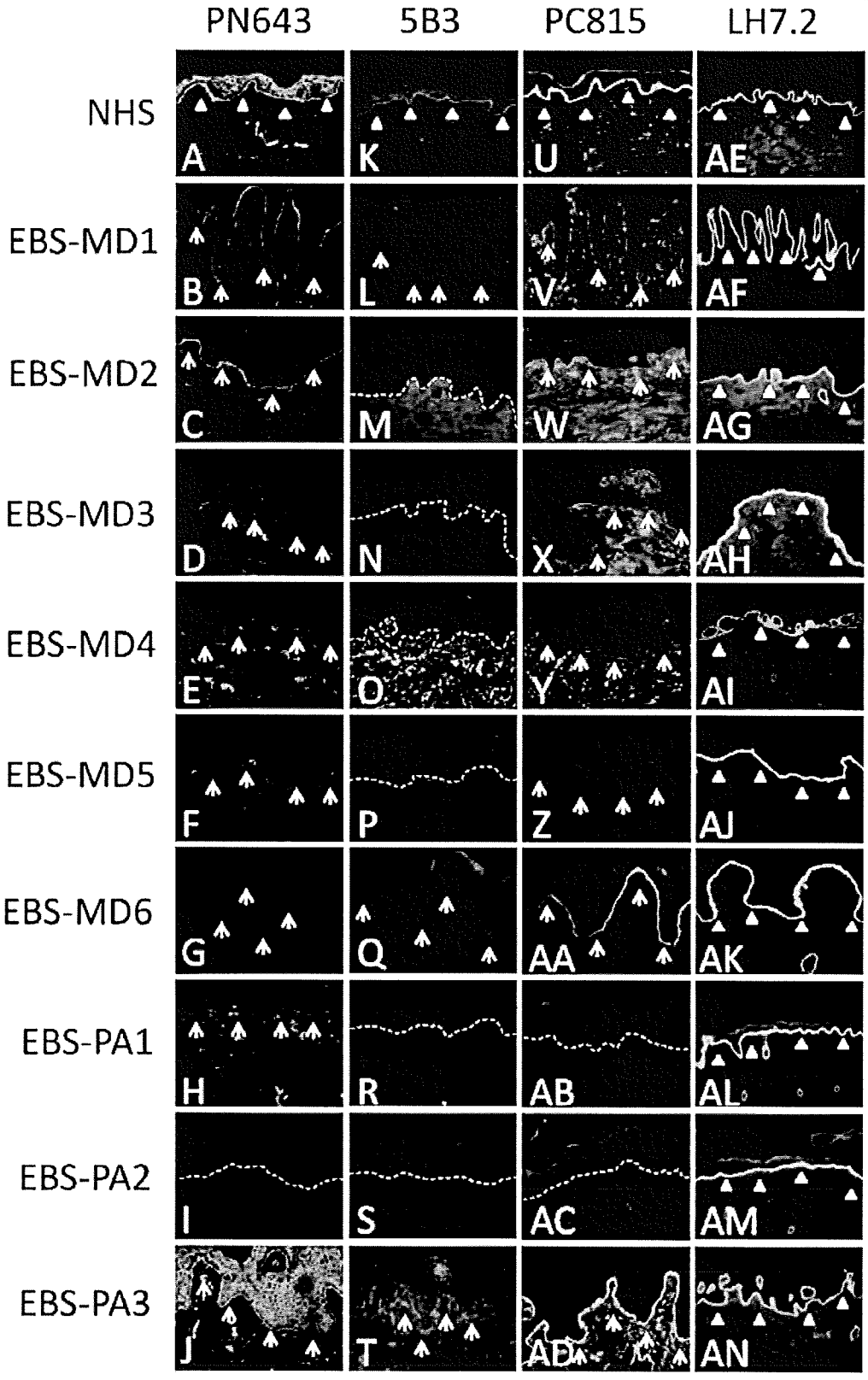

Figure 4. Immunofluorescence analysis of cutaneous plectin expression in EBS-MD and EBS-PA. In normal human skin (NHS), immunofluorescence shows that all mAbs against plectin (PN643, 5B3, and PC815) and type VII collagen (LH7.2) tested in the study bind to the dermal epidermal junction (DEJ) (**A, K, U, AE**). DEJ labeling of PN643 is weakly positive in all EBS-MD cases (**B–G**) and EBS-PA1, 3 (**H, J**), but negative in EBS-PA2 (**I**). DEJ labeling of 5B3 show faintly positive in EBS-MD1, 6 and EBS-PA3 (**L, Q, T**), and negative in EBS-MD2-5 and EBS1, 2 (**M–P, R, S**). DEJ labeling using PC815 is weakly positive in all EBS-MD cases and EBS-PA3 (**V-AA, AD**), but negative in EBS-PA1, 2 (**AB, AC**). Type VII collagen shows normal linear labeling in all EBS cases (**AF–AN**). Strong staining is indicated by arrowheads. Weak labeling is indicated by arrows. Negative labeling is indicated by dotted lines.

revealed loss of full-length plectin with the maintenance of a rodless plectin isoform in EBS-MD. EBS-PA skin specimens harbored greatly reduced amounts of both full-length and rodless plectin.

Protein and mRNA expression patterns of plectin in cultured cells from EBS-MD and EBS-PA patients

Plectin expression patterns of EBS-MD and EBS-PA cultured cells were assessed at both the protein and mRNA levels to confirm the comparative immunofluorescence analysis using skin biopsy specimens showing that the majority of EBS-MD patients expressed a rodless plectin variant, but not full-length plectin and that expression of both full-length and rodless-plectin variant peptides was remarkably reduced or completely abolished in EBS-PA patients. Immunoblot analysis of lysates from fibroblasts of patient EBS-MD5 failed to show any HD1-121 bands, although a band corresponding to rodless plectin was observed by using PN643 and C20 (Fig. 2). Lysates from cultured amniocytes from an aborted sibling of EBS-PA3 (EBS-PA3F) showed that a diminished amount of full-length plectin reacted with PN643, HD1-121, and C20 (Fig. 2).

Using RT-PCR, the presence of an RNA message that does not encode the rod domain was demonstrated in the normal human control as well as the EBS-MD5 and EBS-PA3F cells (Figs. 1C and 5A) (30F/32R). Direct sequencing confirmed the skipping of exon31 in the PCR products (30F/32R) (Fig. 5B). mRNA encoding full-length plectin containing the rod domain was also detected in normal human control, EBS-MD5, and EBS-PA3F cells (Figs. 1C and 5A) (30F/31R and 31F/32R). Judging from the PCR analysis results, the quantity of full-length plectin transcript was greatly reduced in EBS-MD5 and EBS-PA3F compared with those in the normal human controls. In addition, the rodless plectin transcripts were markedly diminished in quantity in EBS-PA3F compared with those of the normal human controls, although expression of the rodless plectin transcripts was maintained in EBS-MD5.

These data suggest that EBS-MD5 fibroblasts express only rodless truncated forms of plectin without the full-length isoform, presumably because of nonsense-mediated mRNA decay (NMD) of the full-length plectin transcript induced by the mutations within *PLEC1* exon 31 (Table 1 and Fig. 1A). Conversely, EBS-PA3F amniocytes expressed a much lower level of plectin than normal human fibroblasts due to NMD of both full-length and rodless plectin transcripts induced by mutations within exons encoding the N-terminal globular domain.

The expression of a small amount of plectin in EBS-PA3 and EBS-PA3F is explained by the splice donor site mutation, c.1344G>A (Table 1 and Fig. 1A). The *PLEC1* cDNA corresponding to exons 9–14 was amplified by PCR using synthesized first-strand cDNA from EBS-PA3F and was cloned into a TA vector. Sequence analysis of the cloned PCR products revealed three different splicing patterns, one of which was a normal transcript from the wild-type allele without c.1344G>A (Fig. 6A and B). In addition to the normal transcript, most of the transcripts derived from the c.1344G>A mutant allele exhibited a 4-bp deletion at nucleotide position 1341–1344 in cDNA (Fig. 6C). This led to a frameshift followed by a PTC at amino acid position 475 (Fig. 6D), whereas small amounts of mRNA exhibiting a

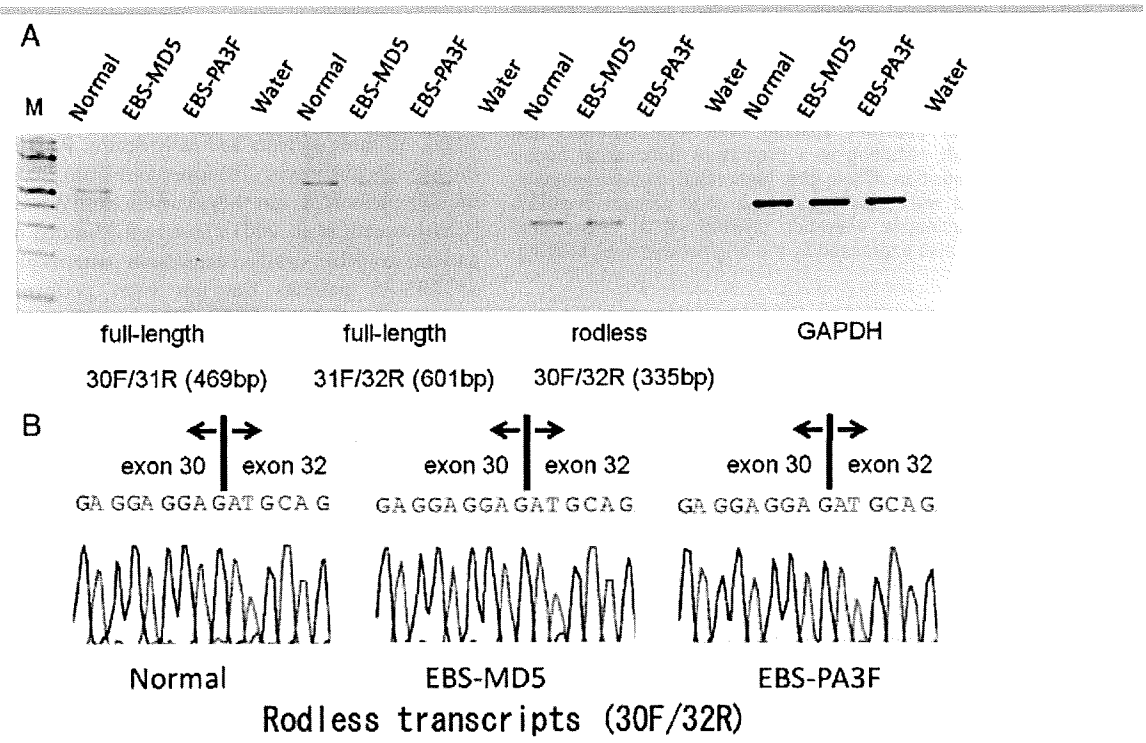

Figure 5. Semiquantitative RT-PCR on full-length and rodless plectin transcripts. **A:** Compared with the normal human control, the EBS-MD5 and EBS-PA3F cells revealed a reduced mRNA level of full-length plectin (30F/31R and 31F/32R). mRNA levels of rodless plectin in EBS-PA3F cells are reduced compared with EBS-MD5 and the normal human control (30F/32R). GAPDH mRNA expression was used as a loading control in these experiments. The negative control reaction (DNA-free water instead of cDNA) shows no PCR products. The molecular weight standard (lane M) is a 100-bp ladder. **B:** Direct sequencing demonstrates skipping of exon 31 in PCR products (30F/32R) from normal human, EBS-MD5, and EBS-PA3F.

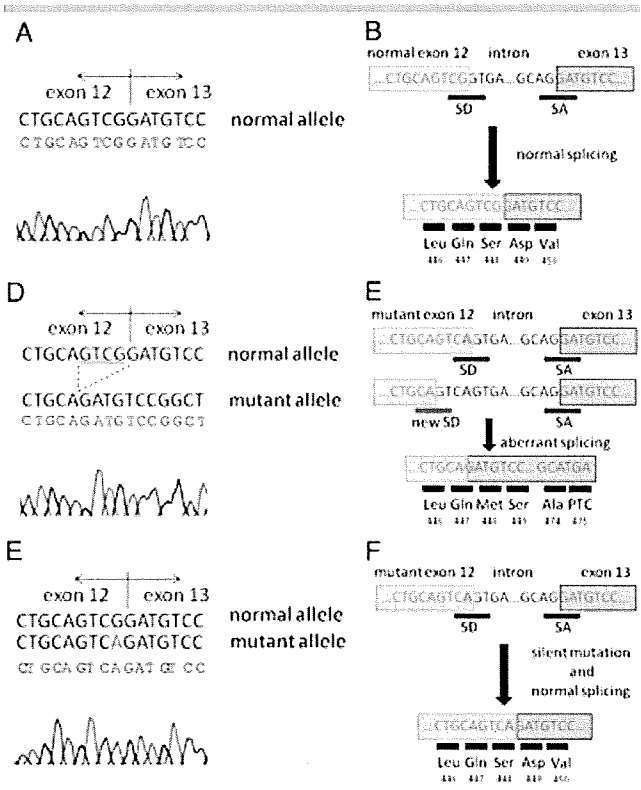

Figure 6. Abnormal splicing due to c.1344G>A mutation in EBS-PA3F, and its consequences **A:** Normal transcripts of the exon 12–exon 13 junction derived from EBS-PA3F cells. **B:** Normal splicing at the exon 12–exon 13 junction. Boxes represent exons, blue underlines are splice sites (SD: splice donor site; SA: splice acceptor site) and black underlined regions are amino acids. **C:** Mutant transcripts with deletion of four nucleotides from exon 12. Deleted nucleotides are underlined. **D:** c.1344G>A mutation altered the G nucleotide of the original splice donor site at the end of exon 12 and activated a cryptic splice donor site (red underline) four nucleotides upstream, leading to aberrant splicing with 4-bp deletion and subsequent frameshift, resulting in a premature termination codon at the amino acid position 475 in the N-terminal globular domain. **E:** Mutant transcripts with c.1344G>A. **F:** A small amount of mRNA carrying a silent nucleotide alteration c.1344G>A at amino acid position 448 Ser was also expressed by the original wild-type splicing.

normal splicing pattern with a silent mutation c.1344G>A at amino acid position 448 Ser were expressed (Fig. 6E and F).

Discussion

This study has demonstrated that two distinct plectin isoforms function in the skin, and that their truncation by *PLEC1* mutations causes the distinct EBS subtypes of EBS-MD and EBS-PA, depending on the pattern of remaining plectin peptide expression.

Plectin has a large rod domain encoded by *PLEC1*exon 31. Alternative splicing of transcripts lacking exon 31 results in a rodless plectin isoform, and it has been demonstrated that the rodless variant is expressed in various rat tissues, including skin, heart, brain, muscle, testis, and liver [Elliott et al., 1997; Fuchs et al., 2005; Steinboeck and Kristufek, 2005]. In addition, the rodless plectin isoform has been found in human muscle cells and keratinocytes [Koster et al., 2004; Schroder et al., 2000]. The significance of this rodless plectin splice variant in the skin remains unclear, but accumulation of *PLEC1* mutational data has revealed that most EBS-MD patients have mutations in exon 31 encoding the large rod domain of plectin, suggesting that conserved expression of the rodless variant plectin could be related to the pathogenesis of EBS-MD in patients with mutations in exon 31 [Pfendner et al., 2005; Sawamura et al., 2007]. However, little data that clarify this hypothesis has been reported, and only one report noted that cultured keratinocytes from one EBS-MD patient were able to express both N- and C-termini plectin epitopes without the expression of rod domain [Koster et al., 2004]. Our data including plectin isoform expression patterns in six EBS-MD patients clearly demonstrate that loss of full-length plectin with conserved rodless plectin isoform expression leads to an EBS-MD phenotype, which is consistent with accumulated clinical and genetic data. We also analyzed the relative amounts of two isoforms of plectin in normal human fibroblasts, keratinocytes, and skeletal muscle (Fig. 3). Our data revealed that the amount of full-length plectin is much greater than that of rodless plectin in fibroblasts and keratinocytes. In contrast, the full-length/rodless ratio in skeletal muscle is a little more than 1. These data are compatible with the fact that EBS-MD patients have skin fragility at birth and develop muscular dystrophy later in life. These data suggests that substantial amounts of rodless plectin in skeletal muscle might delay muscular symptoms while EBS-MD patients are in infancy.

In contrast to the EBS-MD patients, EBS-PA patients are significantly more likely to have mutations in domains outside exon 31 [Pfendner et al., 2005; Sawamura et al., 2007]. The majority of EBS-PA patients included in this study also exhibited *PLEC1* mutations in the gene outside exon 31(Table 1 and Fig. 1A). In the EBS-PA patients in this study, at least one allele is expected to have a stable product (the normal splicing variant from c.1344G>A in EBS-PA1; p.Gln2538X in EBS-PA2, and p.Gln2545X in EBS-PA3). There are three examples in which there are nulls in both alleles that have the PTC outside exon 31 but not in the terminal exon: (1) c.[2727_2740del]+c.[2727_2740del] (exon 22) [Charlesworth et al., 2003], (2) c.[1567_1570del]+c.[1567_1570del] (exon 14) [Pfendner and Uitto, 2005], and (3) p.[Gln305Term]+p.[Gln305Term] (exon 9) [Pfendner and Uitto, 2005]. All three patients had early deaths. Patients (2) and (3) had the EBS-PA phenotype [Pfendner and Uitto, 2005]. Patient (1) had the EBS phenotype, but the occurrence of PA was not substantiated [Charlesworth et al., 2003]. Due to the limited number of EBS-PA patients available, detailed expression patterns of plectin in the skin of EBS-PA patients has not been performed. In addition, comparative analysis of EBS-MD and EBS-PA skin specimens has not been performed. To our knowledge, the present report is the first to compare cutaneous plectin expression in EBS-MD and EBS-PA subtypes using multiple tissues and cells with antibodies that span a range of plectin domains including the N-terminus, rod domain, and C-terminus of plectin. This comparison between EBS-MD and EBS-PA enabled us to identify the differences in these EBS subtypes and to gain a better understanding of the consequences that complete loss or markedly attenuated expression of plectin has. These data are also consistent with the fact that EBS-PA patients generally show more severe skin symptoms than EBS-MD cases, in which expression of a rodless plectin isoform is maintained at least in the skin, although one EBS-PA patient (EBS-PA1) showed a relatively mild skin phenotype [Sawamura et al., 2007]. Also, in some cases of JEB-PA, another subtype of EB with pyloric atresia, the skin manifestations have been reported to be relatively mild and to improve with age, and surgical correction of the PA allowed growth of the patients [Pulkkinen et al., 1998]. It is possible that EBS-PA patients could develop muscular dystrophy if they survived longer. However, to our knowledge, such EBS-PA patients have not been reported in the literature. Figure 7A–C

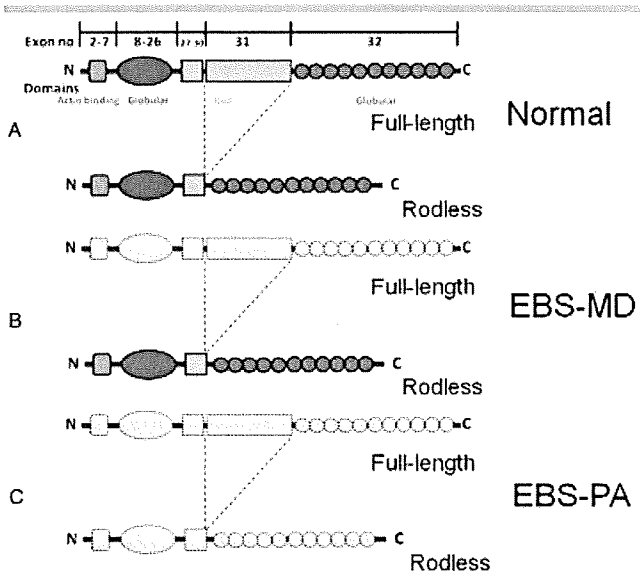

Figure 7. Schematic diagram of cutaneous plectin expression patterns in normal human skin and in skin from EBS-MD and EBS-PA patients. **A:** Two distinct isoforms of plectin—full-length and rodless—are expressed in the normal human control. **B:** Only rodless plectin is expressed in EBS-MD. **C:** Both the full-length and rodless plectin isoforms are greatly diminished or completely lost in EBS-PA. The peptides in light gray are not expressed or are markedly diminished in the patients.

depicts a schematic diagram of the predicted plectin expression pattern among the normal human control, EBS-MD, and EBS-PA.

As described above, almost all EBS-MD patients have one or two truncated mutations in exon 31 encoding the large rod domain of plectin, whereas most *PLEC1* mutations detected in EBS-PA are outside exon 31. To our knowledge, we have three cases of EBS-MD and one case of EBS-PA in the literature whose mutations are not explained by our data: (1) c.[2719_2727del] (exon 21)+c.[2719_2727del] (exon 21) (EBS-MD) [Pulkkinen et al., 1996], (2) c.[1541_1576del] (exon 14)+c.[2677_2685del] (exon 21) (EBS-MD) [Uitto and Pfendner, 2004], (3) c.[2769_2789del] (exon 21)+c.[2769_2789del] (exon 21) (EBS-PA) [Uitto and Pfender, 2005], and (4) c.[13803_13804ins16] (exon 32)+c.[13803_13804ins16] (exon 32) (EBS-MD) [Schroder et al., 2002]. The former three EBS patients had in-frame *PLEC1* deletion mutations outside exon 31 but not in the terminal exon. The last EBS-MD patient was homozygous for out-of-frame mutation in the terminal exon predicting a premature stop-codon within the exon. c.[2719_2727del] was in the nucleotide sequence where CAGGAGGCC was tandemly repeated. Therefore, this in-frame deletion was predicted to result in slipped misparing of DNA [Krawczack and Cooper, 1991; Pfendner and Uitto, 2005]. It is hard to figure out how altered plectin is synthesized from c.[1541_1576del]+c.[2677_2685del] and c.[2769_2789del]+c.[2769_2789del]. It is noteworthy that the phenotype of the EBS-MD patient with c.[1541_1576del]+c.[2677_2685del] was relatively mild, and that muscular dystrophy did not develop until the age of 42 [Uitto and Pfendner, 2004].

In previous studies, the expression of plectin was mainly evaluated by monoclonal antibodies raised against the rod domain. However, several splicing variants had previously prevented us from identifying whether plectin is completely lost or expressed in a truncated protein form in EBS patients with *PLEC1* mutations. Antibodies including those raised against both the plectin N- and C-termini are required to distinguish the expression of rodless splicing variants from a complete protein loss. Nevertheless, we have now elucidated how differences in plectin expression can lead to the two distinct skin blistering-associated phenotypes of muscular dystrophy and pyloric atresia.

Our former study on an EBS-PA3 patient [Nakamura et al., 2005] described different predicted transcripts of the c.1344G>A splice-site mutation from those of the present study. Our previous report employed an exon-trapping system, which is a tool to predict the transcripts that arise from a splice-site mutation when mRNA samples from patient tissues or cells are not available [Buckler et al., 1991]. In that system, the gDNA that is to be screened is subcloned into the exon trapping vector. The subcloned vector is transfected into cells, and mRNA is extracted from the cells to elucidate the splicing consequences. The system is useful, but it is such an artificial way of predicting the splicing products that the induced splicing patterns in the cell culture system are not necessarily correct nor are they the same as those in patient tissues or cultured cells [Schneider et al., 2007]. Because we used cultured amniocytes from EBS-PA3F in the present study, the results shown in Figure 6 supersede the results that were obtained by using an exon-trapping system in the previous report.

To summarize, EBS-MD patients typically express a rodless plectin isoform, although the full-length plectin is lost. In contrast, both full-length and rodless plectin isoforms are deficient in the EBS-PA patients, leading to a more severe disease phenotype. These findings demonstrate that deficiency of both plectin isoforms—full-length and rodless—leads to the severe phenotype of EBS-PA, and in contrast, conserved expression of the rodless isoform results in muscular dystrophy without pyloric atresia. The present results provide important insights toward further understanding the pathomechanisms of muscular dystrophy and pyloric atresia in plectin-deficient patients.

Acknowledgments

We thank Dr. G. Wiche for providing mAb 5B3 and 10F6 and Ms. Yuko Hayakawa for her technical assistance. This work was supported by Health and Labor Sciences Research grants for Research on Measures for Intractable Diseases, from the Ministry of Health, Labor, and Welfare of Japan; by the German EB-Network grant from the Ministry for Education and Research; and by the Excellence Initiative of the German Federal and State Governments (Freiburg Institute for Advanced Studies, FRIAS, School of Life Sciences).

References

Bauer JW, Rouan F, Kofler B, Rezniczek GA, Kornacker I, Muss W, Hametner R, Klausegger A, Huber A, Pohla-Gubo G, Wiche G, Uitto J, Hintner H. 2001. A compound heterozygous one amino-acid insertion/nonsense mutation in the plectin gene causes epidermolysis bullosa simplex with plectin deficiency. Am J Pathol 158:617–625.

Boczonadi V, McInroy L, Maatta A. 2007. Cytolinker cross-talk: periplakin N-terminus interacts with plectin to regulate keratin organisation and epithelial migration. Exp Cell Res 313:3579–3591.

Borradori L, Sonnenberg A. 1999. Structure and function of hemidesmosomes: more than simple adhesion complexes. J Invest Dermatol 112:411–418.

Buckler AJ, Chang DD, Graw SL, Brook JD, Haber DA, Sharp PA, Housman DE. 1991. Exon amplification: a strategy to isolate mammalian genes based on RNA splicing. Proc Natl Acad Sci USA 88:4005–4009.

Charlesworth A, Gagnoux-Palacios L, Bonduelle M, Ortonne JP, De Raeve L, Meneguzzi G. 2003. Identification of a lethal form of epidermolysis bullosa simplex associated with a homozygous genetic mutation in plectin. J Invest Dermatol 121:1344–1348.

Chavanas S, Pulkkinen L, Gache Y, Smith FJ, McLean WH, Uitto J, Ortonne JP, Meneguzzi G. 1996. A homozygous nonsense mutation in the PLEC1 gene in patients with epidermolysis bullosa simplex with muscular dystrophy. J Clin Invest 98:2196–2200.

Dang M, Pulkkinen L, Smith FJ, McLean WH, Uitto J. 1998. Novel compound heterozygous mutations in the plectin gene in epidermolysis bullosa with

muscular dystrophy and the use of protein truncation test for detection of premature termination codon mutations. Lab Invest 78:195–204.

Elliott CE, Becker B, Oehler S, Castanon MJ, Hauptmann R, Wiche G. 1997. Plectin transcript diversity: identification and tissue distribution of variants with distinct first coding exons and rodless isoforms. Genomics 42:115–125.

Fine JD, Eady RA, Bauer EA, Bauer JW, Bruckner-Tuderman L, Heagerty A, Hintner H, Hovnanian A, Jonkman MF, Leigh I, McGrath JA, Mellerio JE, Murrell DF, Shimizu H, Uitto J, Vahlquist A, Woodley D, Zambruno G. 2008. The classification of inherited epidermolysis bullosa (EB): Report of the Third International Consensus Meeting on Diagnosis and Classification of EB. J Am Acad Dermatol 58:931–950.

Fine JD, Eady RA, Bauer EA, Briggaman RA, Bruckner-Tuderman L, Christiano A, Heagerty A, Hintner H, Jonkman MF, McGrath J, McGuire J, Moshell A, Shimizu H, Tadini G, Uitto J. 2000. Revised classification system for inherited epidermolysis bullosa: Report of the Second International Consensus Meeting on diagnosis and classification of epidermolysis bullosa. J Am Acad Dermatol 42:1051–1066.

Foisner R, Feldman B, Sander L, Seifert G, Artlieb U, Wiche G. 1994. A panel of monoclonal antibodies to rat plectin: distinction by epitope mapping and immunoreactivity with different tissues and cell lines. Acta Histochem 96:421–438.

Foisner R, Feldman B, Sander L, Wiche G. 1991. Monoclonal antibody mapping of structural and functional plectin epitopes. J Cell Biol 112:397–405.

Fuchs P, Spazierer D, Wiche G. 2005. Plectin rodless isoform expression and its detection in mouse brain. Cell Mol Neurobiol 25:1141–1150.

Gache Y, Chavanas S, Lacour JP, Wiche G, Owaribe K, Meneguzzi G, Ortonne JP. 1996. Defective expression of plectin/HD1 in epidermolysis bullosa simplex with muscular dystrophy. J Clin Invest 97:2289–2298.

Geerts D, Fontao L, Nievers MG, Schaapveld RQ, Purkis PE, Wheeler GN, Lane EB, Leigh IM, Sonnenberg A. 1999. Binding of integrin alpha6beta4 to plectin prevents plectin association with F-actin but does not interfere with intermediate filament binding. J Cell Biol 147:417–434.

Hieda Y, Nishizawa Y, Uematsu J, Owaribe K. 1992. Identification of a new hemidesmosomal protein, HD1: a major, high molecular mass component of isolated hemidesmosomes. J Cell Biol 116:1497–1506.

Koss-Harnes D, Hoyheim B, Anton-Lamprecht I, Gjesti A, Jorgensen RS, Jahnsen FL, Olaisen B, Wiche G, Gedde-Dahl Jr T. 2002. A site-specific plectin mutation causes dominant epidermolysis bullosa simplex Ogna: two identical de novo mutations. J Invest Dermatol 118:87–93.

Koss-Harnes D, Hoyheim B, Jonkman MF, de Groot WP, de Weerdt CJ, Nikolic B, Wiche G, Gedde-Dahl Jr T. 2004. Life-long course and molecular characterization of the original Dutch family with epidermolysis bullosa simplex with muscular dystrophy due to a homozygous novel plectin point mutation. Acta Derm Venereol 84:124–131.

Koster J, Geerts D, Favre B, Borradori L, Sonnenberg A. 2003. Analysis of the interactions between BP180, BP230, plectin and the integrin alpha6beta4 important for hemidesmosome assembly. J Cell Sci 116(Pt 2):387–399.

Koster J, van Wilpe S, Kuikman I, Litjens SH, Sonnenberg A. 2004. Role of binding of plectin to the integrin beta4 subunit in the assembly of hemidesmosomes. Mol Biol Cell 15:1211–1223.

Krawczak M, Cooper DN. 1991. Gene deletions causing human genetic disease: mechanisms of mutagenesis and the role of the local DNA sequence environment. Hum Genet 86:425–441.

Kunz M, Rouan F, Pulkkinen L, Hamm H, Jeschke R, Bruckner-Tuderman L, Brocker EB, Wiche G, Uitto J, Zillikens D. 2000. Mutation reports: epidermolysis bullosa simplex associated with severe mucous membrane involvement and novel mutations in the plectin gene. J Invest Dermatol 114:376–380.

Laemmli UK. 1970. Cleavage of structural proteins during the assembly of the head of bacteriophage T4. Nature 227:680–685.

Litjens SH, Koster J, Kuikman I, van Wilpe S, de Pereda JM, Sonnenberg A. 2003. Specificity of binding of the plectin actin-binding domain to beta4 integrin. Mol Biol Cell 14:4039–4050.

Litjens SH, Wilhelmsen K, de Pereda JM, Perrakis A, Sonnenberg A. 2005. Modeling and experimental validation of the binary complex of the plectin actin-binding domain and the first pair of fibronectin type III (FNIII) domains of the beta4 integrin. J Biol Chem 280:22270–22277.

McLean WH, Pulkkinen L, Smith FJ, Rugg EL, Lane EB, Bullrich F, Burgeson RE, Amano S, Hudson DL, Owaribe K, McGrath JA, McMillan JR, Eady RA, Leigh IM, Christiano AM, Uitto J. 1996. Loss of plectin causes epidermolysis bullosa with muscular dystrophy: cDNA cloning and genomic organization. Genes Dev 10:1724–1735.

McMillan JR, Akiyama M, Rouan F, Mellerio JE, Lane EB, Leigh IM, Owaribe K, Wiche G, Fujii N, Uitto J, Eady RA, Shimizu H. 2007. Plectin defects in epidermolysis bullosa simplex with muscular dystrophy. Muscle Nerve 35:24–35.

Mellerio JE, Smith FJ, McMillan JR, McLean WH, McGrath JA, Morrison GA, Tierney P, Albert DM, Wiche G, Leigh IM, Geddes JF, Lane EB, Uitto J, Eady RA. 1997. Recessive epidermolysis bullosa simplex associated with plectin mutations: infantile respiratory complications in two unrelated cases. Br J Dermatol 137:898–906.

Nakamura H, Sawamura D, Goto M, Nakamura H, McMillan JR, Park S, Kono S, Hasegawa S, Paku S, Nakamura T, Ogiso Y, Shimizu H. 2005. Epidermolysis bullosa simplex associated with pyloric atresia is a novel clinical subtype caused by mutations in the plectin gene (PLEC1). J Mol Diagn 7:28–35.

Niessen CM, Hulsman EH, Oomen LC, Kuikman I, Sonnenberg A. 1997a. A minimal region on the integrin beta4 subunit that is critical to its localization in hemidesmosomes regulates the distribution of HD1/plectin in COS-7 cells. J Cell Sci 110(Pt 15):1705–1716.

Niessen CM, Hulsman EH, Rots ES, Sanchez-Aparicio P, Sonnenberg A. 1997b. Integrin alpha 6 beta 4 forms a complex with the cytoskeletal protein HD1 and induces its redistribution in transfected COS-7 cells. Mol Biol Cell 8:555–566.

Okumura M, Uematsu J, Hirako Y, Nishizawa Y, Shimizu H, Kido N, Owaribe K. 1999. Identification of the hemidesmosomal 500 kDa protein (HD1) as plectin. J Biochem 126:1144–1150.

Pfendner E, Rouan F, Uitto J. 2005. Progress in epidermolysis bullosa: the phenotypic spectrum of plectin mutations. Exp Dermatol 14:241–249.

Pfendner E, Uitto J. 2005. Plectin gene mutations can cause epidermolysis bullosa with pyloric atresia. J Invest Dermatol 124:111–115.

Pulkkinen L, Rouan F, Bruckner-Tuderman L, Wallerstein R, Garzon M, Brown T, Smith L, Carter W, Uitto J. 1998. Novel ITGB4 mutations in lethal and nonlethal variants of epidermolysis bullosa with pyloric atresia: missense versus nonsense. Am J Hum Genet 63:1376–1387.

Pulkkinen L, Smith FJ, Shimizu H, Murata S, Yaoita H, Hachisuka H, Nishikawa T, McLean WH, Uitto J. 1996. Homozygous deletion mutations in the plectin gene (PLEC1) in patients with epidermolysis bullosa simplex associated with late-onset muscular dystrophy. Hum Mol Genet 5:1539–1546.

Rezniczek GA, de Pereda JM, Reipert S, Wiche G. 1998. Linking integrin alpha6beta4-based cell adhesion to the intermediate filament cytoskeleton: direct interaction between the beta4 subunit and plectin at multiple molecular sites. J Cell Biol 141:209–225.

Rouan F, Pulkkinen L, Meneguzzi G, Laforgia S, Hyde P, Kim DU, Richard G, Uitto J. 2000. Epidermolysis bullosa: novel and de novo premature termination codon and deletion mutations in the plectin gene predict late-onset muscular dystrophy. J Invest Dermatol 114:381–387.

Sawamura D, Goto M, Sakai K, Nakamura H, McMillan JR, Akiyama M, Shirado O, Oyama N, Satoh M, Kaneko F, Takahashi T, Konno H, Shimizu H. 2007. Possible involvement of exon 31 alternative splicing in phenotype and severity of epidermolysis bullosa caused by mutations in PLEC1. J Invest Dermatol 127:1537–1540.

Schaapveld RQ, Borradori L, Geerts D, van Leusden MR, Kuikman I, Nievers MG, Niessen CM, Steenbergen RD, Snijders PJ, Sonnenberg A. 1998. Hemidesmosome formation is initiated by the beta4 integrin subunit, requires complex formation of beta4 and HD1/plectin, and involves a direct interaction between beta4 and the bullous pemphigoid antigen 180. J Cell Biol 142:271–284.

Schneider B, Koppius A, Sedlmeier R. 2007. Use of an exon-trapping vector for the evaluation of splice-site mutations. Mamm Genome 18:670–676.

Schroder R, Furst DO, Klasen C, Reimann J, Herrmann H, van der Ven PF. 2000. Association of plectin with Z-discs is a prerequisite for the formation of the intermyofibrillar desmin cytoskeleton. Lab Invest 80:455–464.

Schröder R, Kunz WS, Rouan F, Pfendner E, Tolksdorf K, Kappes-Horn K, Altenschmidt-Mehring M, Knoblich R, van der Ven PF, Reimann J, Fürst DO, Blümcke I, Vielhaber S, Zillikens D, Eming S, Klockgether T, Uitto J, Wiche G, Rolfs A. 2002. Disorganization of the desmin cytoskeleton and mitochondrial dysfunction in plectin-related epidermolysis bullosa simplex with muscular dystrophy. J Neuropathol Exp Neurol 61:520–530.

Smith FJ, Eady RA, Leigh IM, McMillan JR, Rugg EL, Kelsell DP, Bryant SP, Spurr NK, Geddes JF, Kirtschig G, Milana G, de Bono AG, Owaribe K, Wiche G, Pulkkinen L, Uitto J, McLean WH, Lane EB. 1996. Plectin deficiency results in muscular dystrophy with epidermolysis bullosa. Nat Genet 13:450–457.

Sonnenberg A, Liem RK. 2007. Plakins in development and disease. Exp Cell Res 313:2189–2203.

Steinboeck F, Kristufek D. 2005. Identification of the cytolinker protein plectin in neuronal cells—expression of a rodless isoform in neurons of the rat superior cervical ganglion. Cell Mol Neurobiol 25:1151–1169.

Takahashi Y, Rouan F, Uitto J, Ishida-Yamamoto A, Iizuka H, Owaribe K, Tanigawa M, Ishii N, Yasumoto S, Hashimoto T. 2005. Plectin deficient epidermolysis bullosa simplex with 27-year-history of muscular dystrophy. J Dermatol Sci 37:87–93.

Takizawa Y, Shimizu H, Rouan F, Kawai M, Udono M, Pulkkinen L, Nishikawa T, Uitto J. 1999. Four novel plectin gene mutations in Japanese patients with epidermolysis bullosa with muscular dystrophy disclosed by heteroduplex scanning and protein truncation tests. J Invest Dermatol 112:109–112.

Uitto J, Pfendner E. 2004. Compound heterozygosity of unique in-frame insertion and deletion mutations in the plectin gene in a mild case of epidermolysis bullosa with very late onset muscular dystrophy. J Invest Dermatol 122:A86.

Varki R, Sadowski S, Pfendner E, Uitto J. 2006. Epidermolysis bullosa. I. Molecular genetics of the junctional and hemidesmosomal variants. J Med Genet 43:641–652.

Wiche G. 1998. Role of plectin in cytoskeleton organization and dynamics. J Cell Sci 111(Pt 17):2477–2486.

European Journal of Human Genetics (2010) 18, 26–32

www.nature.com/ejhg

ARTICLE

Novel *IL31RA* gene mutation and ancestral *OSMR* mutant allele in familial primary cutaneous amyloidosis

Ming-Wei Lin*[,1,2,12], Ding-Dar Lee[3,4,12], Tze-Tze Liu[5], Yong-Feng Lin[6], Shang-Yi Chen[1], Chih-Cheng Huang[7], Hui-Ying Weng[7], Yu-Fen Liu[5], Akio Tanaka[8], Ken Arita[8,9], Joey Lai-Cheong[8], Francis Palisson[10], Yun-Ting Chang[3,4], Chu-Kwan Wong[3], Isao Matsuura[11], John A McGrath[8] and Shih-Feng Tsai*[,5,6,11]

Primary cutaneous amyloidosis (PCA) is an itchy skin disorder associated with amyloid deposits in the superficial dermis. The disease is relatively common in Southeast Asia and South America. Autosomal dominant PCA has been mapped earlier to 5p13.1–q11.2 and two pathogenic missense mutations in the *OSMR* gene, which encodes the interleukin-6 family cytokine receptor oncostatin M receptor beta (OSMRβ), were reported. Here, we investigated 29 Taiwanese pedigrees with PCA and found that 10 had heterozygous missense mutations in *OSMR*: p.D647V (one family), p.P694L (six families), and p.K697T (three families). The mutation p.P694L was associated with the same haplotype in five of six families and also detected in two sporadic cases of PCA. Of the other 19 pedigrees that lacked *OSMR* pathology, 8 mapped to the same locus on chromosome 5, which also contains the genes for 3 other interleukin-6 family cytokine receptors, including interleukin-31 receptor A (IL31RA), which can form a heterodimeric receptor with OSMRβ through interleukin-31 signaling. In one family, we identified a point mutation in the *IL31RA* gene, c.1562C>T that results in a missense mutation, p.S521F, which is also sited within a fibronectin type III-like repeat domain as observed in the *OSMR* mutations. PCA is a genetically heterogeneous disorder but our study shows that it can be caused by mutations in two biologically associated cytokine receptor genes located on chromosome 5. The identification of *OSMR* and *IL31RA* gene pathology provides an explanation of the high prevalence of PCA in Taiwan as well as new insight into disease pathophysiology.
European Journal of Human Genetics (2010) **18,** 26–32; doi:10.1038/ejhg.2009.135; published online 19 August 2009

Keywords: primary cutaneous amyloidosis; *OSMR*; *IL31RA*; genetic heterogeneity; haplotype

INTRODUCTION

Primary cutaneous amyloidosis (PCA) is a relatively common itchy skin disorder in South America and Southeast Asia.[1–3] The disease is characterized histologically by focal deposition of amyloid in the dermal papillae of lesional skin. The precise pathogenesis of PCA is unclear, but it is considered to be multifactorial, involving both genetic and environmental contributions. Earlier reports have implicated frictional epidermal damage,[4] apoptosis,[5] viral infection,[6] and other triggers in the disease etiology.

Most PCA cases are sporadic, although a significant proportion of patients from certain geographical areas may have an autosomal dominant pattern of inheritance.[7–18] Notably, Ollague *et al*[2] reported that about one-third of the cases of PCA in South America have a positive family history. In Southeast Asia, familial PCA (FPCA) is also prevalent, especially in Chinese families, more so than in Malays and Indians.[3] Thus, familial aggregation and differing racial susceptibilities suggest that genetic factors may have a significant role in the pathogenesis of FPCA.

Our group has reported 56 cases of PCA with a positive family history.[19] Using a candidate gene approach, we reported earlier possible linkage to chromosome 1q23.[20] Subsequently, however, we showed significant linkage of FPCA to a different locus on chromosome 5p13.1–q11.2 using a genome-wide scan with microsatellite markers.[21] Further analysis, focusing on two large Taiwanese families with FPCA, identified a common haplotype shared by all affected individuals located between D5S1490 and D5S623.

Within this critical region, Arita *et al*[22] have replicated the linkage data for chromosome 5p13.1–q11.2 in a large Brazilian family. Moreover, they identified a missense mutation (c.2072T>C; p.I691T) in all affected individuals in the *OSMR* gene, encoding oncostatin M-specific receptor β (OSMRβ). Additional studies in two other white families from the United Kingdom and South

[1]Institute of Public Health, National Yang-Ming University, Taipei, Taiwan; [2]Department of Medical Research and Education, Taipei Veterans General Hospital, Taipei, Taiwan; [3]Department of Dermatology, Taipei Veterans General Hospital, Taipei, Taiwan; [4]Department of Dermatology, Faculty of Medicine, National Yang-Ming University, Taipei, Taiwan; [5]Genome Research Center, National Yang-Ming University, Taipei, Taiwan; [6]Department of Life Sciences and Institute of Genome Sciences, National Yang-Ming University, Taipei, Taiwan; [7]Institute of Biomedical Informatics, National Yang-Ming University, Taipei, Taiwan; [8]St John's Institute of Dermatology, King's College London (Guy's campus), London, UK; [9]Department of Dermatology, Hokkaido University School of Medicine, Sapporo, Japan; [10]Facultad de Medicina Clinica Alemana, Universidad del Desarrollo, Santiago, Chile; [11]Division of Molecular and Genomic Medicine, National Health Research Institutes, Miaoli, Taiwan
[12]These authors contributed equally to this work.
*Correspondence: Dr M-W Lin, Institute of Public Health, National Yang-Ming University, No. 155, Section 2, LiNong Street, Beitou, Taipei 112, Taiwan. Tel: +886 2 2826 7379; Fax:+886 2 2821 0514; E-mail: mwlin@ym.edu.tw and Professor S-F Tsai, Division of Molecular and Genomic Medicine, National Health Research Institutes, 35 Keyan Rd, Zhunan Town, Miaoli County 350, Taiwan. Tel: +886 37 246166 Ext 35310; Fax:+886 37 586459; E-mail: petsai@nhri.org.tw
Received 17 February 2009; revised 4 June 2009; accepted 26 June 2009; published online 19 August 2009

Africa discovered another heterozygous missense mutation (c.1853G>C; p.G618A) common to the affected individuals in both pedigrees, thus establishing *OSMR* as a disease gene for some cases of FPCA.[22]

The *OSMR* gene belongs to the interleukin-6 (IL-6) cytokine receptor gene family. Cytokines of the IL-6 family include IL-6, IL-11, IL-27, and IL-31, ciliary neurotrophic factor, cardiotrophin-1, cardiotrophin-like cytokine, leukemia inhibitory factor, neuropoietin, and OSM.[23] IL-6-type cytokines exert their action through the signal transduction leading to the activation of the JAK/STAT, MAPK, and PI3K/Akt cascades.[24] Several cytokine receptors have been reported to be structurally similar to but functionally distinct from the prototype IL-6 receptor, which consists of two gp130 and one IL-6R molecule. In the OSM type I receptor, leukemia inhibitory factor receptor (LIFR) heterodimerizes with gp130, whereas in the OSM type II receptor, OSMRβ with gp130. Furthermore, OSMRβ couples with the IL-31 receptor A subunit to constitute the IL-31 receptor. Notably, four genes encoding the IL-6-type receptor components are located in chromosome 5: *LIFR* (38.510–38.592 Mb), *OSMR* (38.881–38.970 Mb), *IL31RA* (55.183–55.248 Mb), and *IL6ST* (55.272–55.326 Mb), encoding LIFR, OSMRβ, IL-31 receptor A, and gp130, respectively.

To investigate the genetic basis of FPCA in Taiwan, we sequenced *OSMR* in families that mapped to 5p13.1–q11.2 and defined the genetic backgrounds in these cases that contribute to the high prevalence of PCA in Taiwan. To further characterize the possible genetic heterogeneity observed in our collection of FPCA pedigrees,[16] we also used the Affymetrix GeneChip Human Mapping 10K Array to conduct a whole-genome scan on nine pedigrees that showed earlier weak positive linkage. On the basis of linkage analysis, we further investigated gene mutations in the chromosome 5 critical region and identified mutations in two genes related to the IL-6 cytokine pathway. Moreover, we have identified specific chromosome 5 haplotypes that are associated with new and recurrent mutations in the *OSMR* gene.

MATERIALS AND METHODS

Study subjects

Genomic DNA samples from 29 families showing autosomal dominant form of PCA were available for this study. Fifteen of these pedigrees were analyzed earlier in a published genome-wide linkage analysis, and a significant linkage region was mapped to chromosome 5p13.1–q12.1 in some, but not all, pedigrees.[21] Of the other 14 families, 7 have at least two subjects affected with PCA and these were included for linkage replication. Taken together, the 29 multiplex families contained 73 affected individuals and 69 phenotypically normal subjects. In addition, we also collected DNA from 91 sporadic PCA subjects, including 23 singleton trio families and 68 affected individuals (Figure 1). As controls, 142 clinically unaffected subjects were recruited for this study. Each participant was examined by a dermatologist to determine the disease status of PCA. The diagnosis of PCA was made based on the typical clinical pictures of the skin lesions. For those cases whose clinical pictures were ambiguous, skin biopsies were performed to confirm the diagnosis.

Genotyping and linkage replication study

A 10-ml whole blood sample was taken from each individual for DNA analysis. Genomic DNA was extracted using Puregen kit (Gentra Systems, Minneapolis, MN, USA) according to the manufacturer's instructions. Seven microsatllites (D5S1993, D5S426, D5S1490, D5S418, D5S623, D5S1969, and D5S407), spanning the significant linkage region on chromosome 5, were selected for genotyping to replicate our previous linkage findings. PCR amplification, electrophoresis, and data analysis were carried out as reported earlier.[21]

Genotyping with the Affymetrix GeneChip Human Mapping 10K Array

As microsatellite-based genome scan set may not provide adequate marker density for certain chromosomal regions, the Affymetrix GeneChip Human Mapping 10K Array with an average density between SNPs of 0.32 cM (210 kb) was also performed on nine FPCA families (B, E, G, I, J, K, L, N, P). DNA labeling, hybridization, washing, and staining of 10K SNP arrays were performed according to the manufacturer's protocol (Affymetrix Inc., Santa Clara, CA, USA). The 10 K SNP mapping data were analyzed with the Affymetrix GeneChip DNA Analysis Software (GDAS) to generate genotype calls for each of the SNP probes on the array.

Sequencing of the *OSMR*, *IL31RA*, and *IL6ST* genes

We sequenced the *OSMR* gene in 306 individuals, including 73 individuals from PCA families, 91 cases of sporadic PCA, and 142 control subjects. Direct PCR sequencing was used to examine the promoter region and all 18 exons and flanking introns of the *OSMR* gene, using 20 pairs of primers. As for the *IL31RA* gene, we sequenced 24 individuals from PCA families, 91 cases of sporadic PCA, and 142 control subjects by examining all exons and flanking introns of the *IL31RA* gene using 21 pairs of primers for nine splice isoforms of IL31RA. We also sequenced the *IL6ST* gene in 22 individuals from PCA families and two cases of sporadic PCA by using 18 pairs of primers for two splice isoforms of IL6ST (NM_002184 and NM_175767). Detailed information of primer sequences is available on request. The sequencing reactions were performed using the ABI BigDye Terminator reagents and were electrophorezed

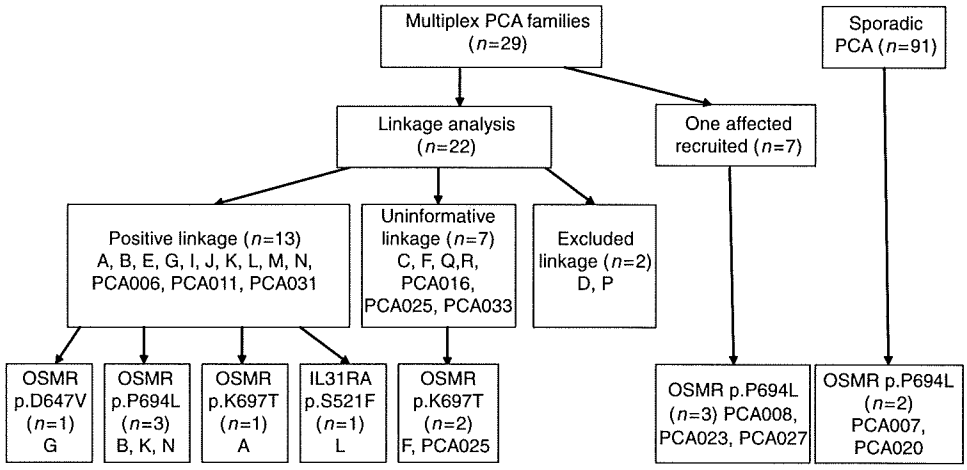

Figure 1 Outline of subject recruitment, linkage results, and mutation findings. DNA samples were collected from affected and unaffected individuals to investigate the genetic causes of PCA.

on the ABI PRISM 3730 DNA sequencer (Applied Biosystems, Foster City, CA, USA). The sequence data were analyzed by using the PolyPhred software (v5.04).[25]

Genotyping with the Illumina Human CNV370-Duo DNA Analysis BeadChip

Genome-wide genotyping on 75 Taiwanese subjects, including 23 PCA subjects, was performed with the Illumina Human CNV370-Duo DNA Analysis BeadChip (Illumina, San Diego, CA, USA). We also applied the same procedure to determine the genotypes for selected targets on chromosome 5 for seven individuals of one PCA family from Chile (see mutation data results below). The chip contains 318 237 haplotype tagging SNPs, with an additional 52 167 markers designed to specifically target nearly 14 000 copy number variant (CNV) regions of the genome, for a total of 370 404 markers. Genotyping was performed according to the manufacturer's protocols.

Haplotype and statistical analysis

We investigated and compared the haplotype structure for the chromosome 5 region containing the genes for four cytokine receptors (*LIFR, OSMR, IL31RA, IL6ST*), using genotype data of the International HapMap Project (http://www.hapmap.org).[26]

Two-point and multipoint linkage analysis was conducted using the MLINK and LINKMAP options of the LINKAGE packages v5.1, respectively (ftp://linkage.rockefeller.edu/software/linkage).[27] Multipoint lod score, non-parametric linkage, and haplotype construction were performed by the GENEHUNTER program v2.5 (http://www.broad.mit.edu/ftp/distribution/software/genehunter/).[28]

The Haploview software v4. 0 (www.broad.mit.edu/personal/jcbarret/haploview/) was used for halpotype block identification, and haplotype association test.[29] The GENECOUNTING program v2.1 (http://www.mrc-epid.cam.ac.uk/Personal/jinghua.zhao/software/) was used for estimating the frequencies of haplotypes in different haplotype blocks.[30–31] *P*-values less than 0.01 were considered to be statistically significant.

RESULTS

Linkage replication study

In the initial genome-wide scan, we conducted genotype analysis on 15 families and identified 10 pedigrees (A, B, E, G, I, J, K, L, M, N) that showed positive linkage to the chromosome 5 markers.[21] On this basis, we recruited seven additional pedigrees for linkage replication (see Figure 1 for details of pedigrees/individuals studied). Three of them (PCA006, PCA011, PCA031) gave positive lod scores, with a maximum multipoint lod score of 1.07 for the marker D5S623. The remaining four pedigrees (R, PCA016, PCA025, PCA033), however, showed no evidence of linkage because of small size of the pedigrees. Nevertheless, when we combined these seven pedigrees with the 15 pedigrees from our initial study for linkage analysis, a maximum heterogeneity lod score of 5.10 (α=0.60) was found for the marker D5S623 (Supplementary Table 1).

The Affymetrix 10K Array was also used for genome-wide linkage scan on nine families. This alternative mapping tool helped identify one family (pedigree J) that had a positive lod score of 1.81. Furthermore, additional regions giving lod>1 were detected for chromosomes 2, 11, 15, 16, and 21 with the SNP markers (Supplementary Table 2).

OSMR mutations in PCA

We applied PCR sequencing to screen exonic mutation in the *OSMR* gene in PCA patients. As shown in Table 1 and Figure 1, we identified three new heterozygous mutations in the *OSMR* gene in the Taiwanese patients. One mutation, c.2081C>T (p.P694L), was identified in six FPCA pedigrees, whereas the mutation c.2090A>C (p.K697T) was found in three families and a third mutation (c.1940A>T; p.D647V) was detected in one pedigree. Interestingly, the p.P694L mutation was also detected in two Taiwanese sporadic cases, who had reported earlier no other affected individual in their families. We also identified this mutation in a Chilean family with FPCA (unreported data). None of the 142 control subjects from Taiwan (or over 250 control chromosomes from other populations) showed presence of p.P694L or the other missense mutations. All these amino-acid substitutions occur within the fibronectin III-like domains of OSMRβ, in a similar location to the mutations reported by Arita *et al.*[22] No mutations in *OSMR* were identified in the other 19/29 pedigrees, including eight pedigrees that showed linkage to the chromosome 5 interval.

Table 1 ***OSMR*** **mutations in Taiwan**

Location	*Nucleotide*	*Codon*	*Familial PCA* n=*73*	*Sporadic PCA* n=*91*	*Control* n=*142*
Exon 14	c.1940A>T	p.D647V	3 (4.1%)	0 (0.0%)	0 (0.0%)
Exon 15	c.2081C>T	p.P694L	20 (27.4%)	2 (2.2%)	0 (0.0%)
Exon 15	c.2090A>C	p.K697T	4 (5.5%)	0 (0.0%)	0 (0.0%)

Haplotype block structure of the *OSMR* region

To define the genetic backgrounds that are associated with the recurrent *OSMR* mutations in Taiwan, we conducted haplotype analysis on affected individuals from the multiplex families using the Illumina Human CNV370-Duo DNA Analysis BeadChip array. This array contains 370 404 probes and it can detect 21 068 SNP variations located on human chromosome 5. One representative case from each of the six families with the p.P694L mutation (B, K, N, PCA008, PCA023, PCA027), the three families with the p.K697T mutation (A, F, PCA025), the single family with the p.D647V mutation (G), as well as from the eight families with no detectable *OSMR* gene mutation (C, E, I, J, L, M, Q, PCA006) (Figure 1) was selected for genotype analysis. On the basis of haplotype block deduced from the genotype data of Taiwanese individuals, we investigated, in different populations, the haplotype block patterns of the region on chromosome 5 containing the genes for four cytokine receptors (*LIFR, OSMR, IL31RA, IL6ST*) (Supplementary Figure 1a and 1b). For reference, SNP genotype data from 52 other Taiwainese (non-PCA family subjects) were also collected for haplotype analysis. Using the combined genotype data of the controls and the PCA patients, 37 and 32 blocks could be identified for the Taiwanese population in the regions covering *LIFR-OSMR* genes (38–39.5 Mb) and *IL31RA-IL6ST* genes (54.5–56 Mb), respectively. Haplotype analysis showed that blocks 4 and 25 in the region of the *LIFR–OSMR* genes produced significant results with *P*-values of 0.0007, and 0.0080, respectively. Another two blocks (21 and 30) in the region of the *IL31RA–IL6ST* genes were also found to differ significantly between PCA cases and controls (*P*-values=0.0099 and 0.0022, respectively).

Haplotypes associated with *OSMR* mutations

We then investigated whether the recurrent *OSMR* mutations in Taiwanese subjects are associated with specific chromosome 5 haplotypes. If so, this could indicate a common ancestor for all the respective families. Using the haplotype block information deduced from the genotype data, we investigated the chromosome 5 region containing the genes for four cytokine receptors (*LIFR, OSMR, IL31RA, IL6ST*) and looked for haplotypes that were associated with the *OSMR* mutations. As shown in the Table 2, we focused on four haplotype blocks, 4, 25, 21, 30, and found that the 4-AACC and

Table 2 Haplotypes associated with *OSMR* mutations

Genomic region	Block number	Associated haplotype	With mutation p.P694L (n=12)	With mutation p.K697T (n=6)	With mutation p.D647V (n=2)	No detectable mutation (n=16)	Control (n=104)	P-value
38–39.5 Mb	4[a]	AACC	3 (25.0%)	3 (50.0%)	—	2 (12.5%)	4 (3.8%)	0.001
	25[b]	GAAAA	5 (41.7%)	—	—	—	2 (1.9%)	0.00041
54.5–56 Mb	21[c]	CGGG	1 (8.3%)	2 (33.3%)	—	3 (18.8%)	4 (3.8%)	0.023
	30[d]	CC	4 (33.3%)	—	—	2 (12.5%)	3 (2.9%)	0.006

[a]Defined by rs10512674, rs270592, rs10055239, and rs1494645.
[b]Defined by rs386994, rs451298, rs1501742, rs3805558, and rs420444.
[c]Defined by rs286007, rs11741905, rs286002, and rs158214.
[d]Defined by rs4129542 and rs4700382.

21-CGGG haplotypes were overrepresented in the group with the mutation p.K697T, whereas the 25-GAAAA and 30-CC haplotypes were overrepresented in the group with the mutation p.P694L. The association between the 25-GAAAA haplotype and the mutation p.P694L was striking; affected individuals from five of six families with the mutation p.P694L carried this haplotype. Moreover, we could confirm this association in two sporadic PCA cases (PCA007-1 and PCA020-1) that were found to have the mutation p.P694L (Figure 1): both of them had the 25-GAAAA haplotype. Taken together, our data indicate that a major proportion of PCA from Taiwan associated with the mutation p.P694L originates from the same specific chromosome background represented by the 25-GAAAA haplotype. We then went on to determine the haplotypes for members of an FPCA pedigree from Chile some of which also harbored the mutation p.P694L. As shown in Figure 2a, the affected individuals (80, 82 and 252) in this family were found to have the clinical manifestation of PCA. We found that the three Chilean individuals carrying the *OSMR* mutation have the same haplotypes of 4-CATC, 25-GGAGA, 21-CGAG, and 30-CC. Comparison with the Taiwanese data indicates that the Chilean FPCA has occurred on different genetic backgrounds.

We also encountered a unique pedigree originated from Taiwan, in which both parents and their two sons were all diagnosed with PCA (Figure 2b). To trace the genetic origin(s) of PCA in the family, we conducted genotyping and sequencing to identify the mutant allele(s) associated with the disease for each patient. SNP genotyping showed that the mother (individual 7) and one affected son (individual 10) carried the prototypic haplotype of the p.P694L mutation and DNA sequence confirmed the presence of the mutation. On the other hand, the father (individual 8) and the other affected son (individual 11) did not have this *OSMR* mutation or the associated haplotype (or indeed any other *OSMR* mutation). Thus, the data indicate that two different genes were involved in the PCA etiology of this family. Interestingly, we noticed that those who have p.P694L mutation showed greater severity of PCA. Although all four patients presented typical clinical pictures, individuals 7 and 10 had larger areas of skin lesion (upper back, forearms, thighs, and lower legs) and a higher density of amyloid papules, as compared with those without the mutation (individuals 8 and 11).

IL31RA mutation in FPCA

So far we have found *OSMR* coding mutation in 5 out of the 13 pedigrees that showed linkage to the chromosome 5 region. We also investigated the other two cytokine genes (*IL31RA*, *IL6ST*) for sequence change in the other eight families that mapped to the chromosome 5 region. No alteration was found in the coding sequence of *IL6ST* for these eight families. However, as indicated in Figure 3, a p.S521F mutation (c.1562C>T, codon 521 TCT>TTT) was found in the *IL31RA* gene in a FPCA family. The p.S521F variation was detected in the affected individual but not found in unaffected individual in Pedigree L. This variant neither exists in other PCA patients nor in 142 controls we examined, and the codon change occurs in a codon position that is well conserved in mammals (Supplementary Figure 2). No other alteration was identified in the coding sequence and exon/intron boundary except a cSNP at codon 529 (p.S529N, c.1586G>A, in dbSNP: rs161704) for this family.

DISCUSSION

Clinically, it is evident that PCA is a common disease in Taiwan and South America. Although environmental factors may have contributed to the high PCA prevalence in these regions, we have taken a genetic approach and identified chromosomal backgrounds that are uniquely associated with the disease in Taiwan. In this study, we have identified three new mutations in the *OSMR* gene that underlie PCA. Moreover, we have found out that *IL31RA*, another gene mapped to the same chromosome and functionally related to the IL-6 cytokines, is involved in FPCA. Two recurrent mutations (p.P694L and p.K697T) are located in exon 15, whereas the other mutation, p.D647V, occurs in exon 14 of the *OSMR* gene. Including the published p.G618A and p.I691T mutations reported by Arita *et al*,[22] substitutions of five different highly conserved amino-acid residues in the fibronectin III-like domains of OSMRβ have now been determined as the molecular basis of FPCA. As shown in Figure 4a and 4b, the mutations reported in this paper are all located in the fibronectin III-like domains of OSMRβ and IL-31RA. Earlier studies have indicated that these particular domains are critical for receptor dimerization for both gp130 homodimers and gp130-LIFR heterodimers.[32–33] Therefore, Arita *et al*[22] have proposed that the amino-acid substitutions in the fibronectin type III-like domain may interfere with receptor coupling of OSMRβ with gp130 or OSMRβ with IL31RA. Another effect of the pathogenic *OSMR* mutations could be premature degradation of the mutant proteins leading to reduced availability of OSMRβ to interact with either gp130 or IL31RA. Although the precise cellular mechanism of PCA pathogenesis remains to be established, Arita *et al*[22] have shown, in cultured keratinocytes from FPCA patients, decreased phosphory-
lation of STATs, Erk1/2, and Akt after OSM stimulation, and no phosphorylation after IL-31 stimulation. Thus, mutations involving members of the IL-6 receptor gene family can cause dysfunction of the downstream signals and lead to the development of cutaneous diseases, here manifesting as FPCA.

Data from the linkage analyses have provided new evidence that FPCA is genetically heterogeneous. As well as other putative genes within the region of linkage on chromosome 5 being possible candidate genes in some pedigrees (including other IL-6 family cytokine receptors), other undisclosed loci may be relevant to disease

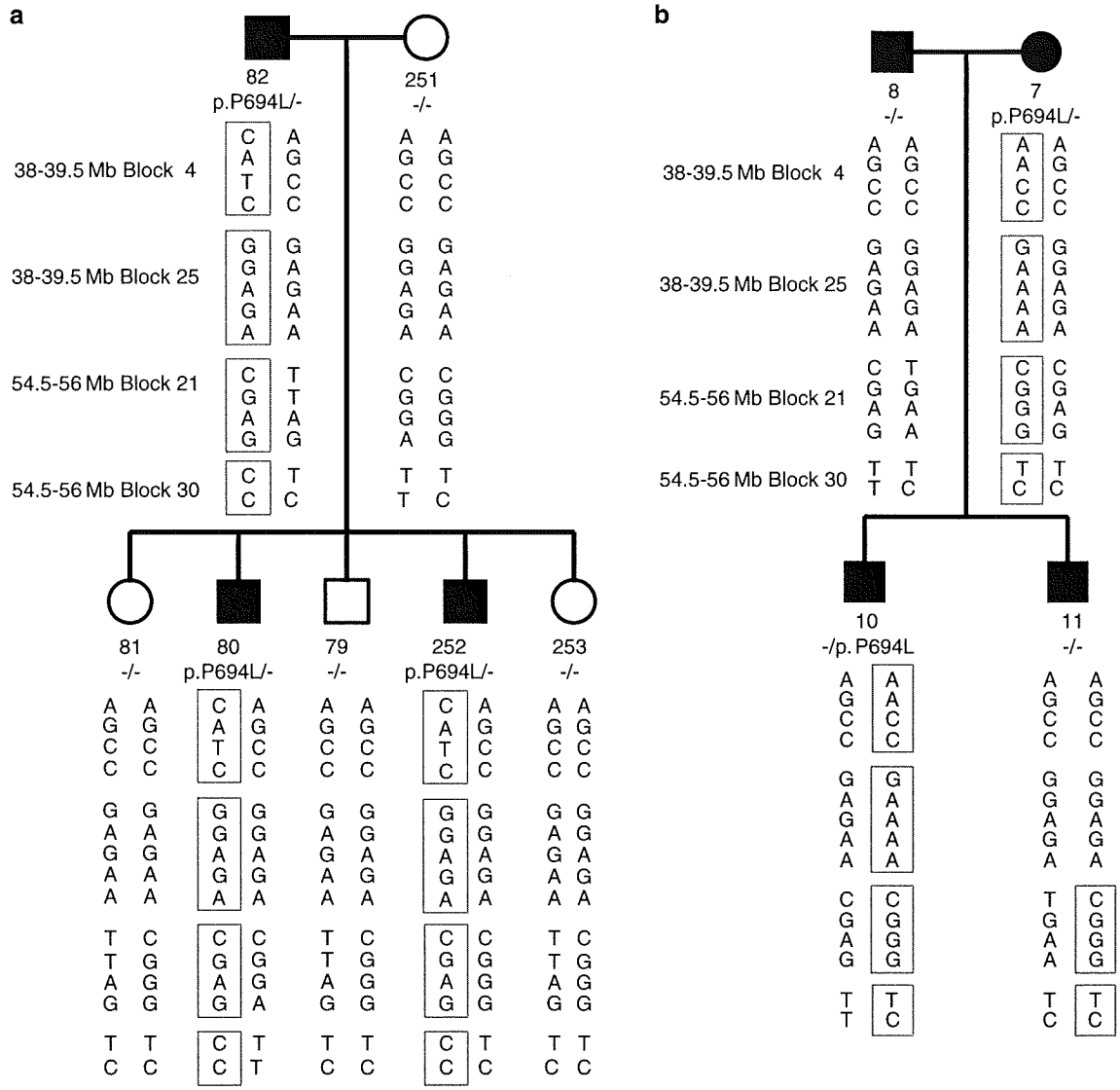

Figure 2 Haplotype analysis of a Chilean family and a Taiwanese family with the *OSMR* mutation p.P694L. **(a)** Three individuals of the Chilean family, including individuals 82, 80, and individual 252, have the clinical manifestation of PCA and were found to share the same haplotypes. **(b)** All four individuals of the Taiwanese family had clinical manifestation of PCA. However, only two (individual 7 and individual 10) were found to share the same haplotypes. In individual 11, the paternal allele was marked with 4-AGCC, 25-GGAGA, 21-TGAA, and 30-TC, and the maternal allele was determined to be a recombinant of the two alleles from the mother.

pathogenesis. Of note, two families (D and P) gave negative lod scores, and as such the FPCA in these cases is likely to be caused by genes outside the chromosome 5 region. Consistent with our knowledge of the complex signaling pathways elicited by the IL-6-related cytokines (IL-6, IL-31, and OSM) and the now-proven genetic heterogeneity, the pedigree analyzed in Figure 2b illustrates that FPCA can be traced to different genetic causes even within the same family.

In this study, we have shown that the recurrent *OSMR* mutation p.P694L is present on similar chromosomal backgrounds (haplotypes) in several Taiwanese families with FPCA. We have also analyzed the *OSMR* sequence in 91 sporadic PCA and identified 2 cases (PCA007 and PCA020) with the same mutation and the same haplotype. It is likely, therefore, that these two subjects and those in five of the six families with this mutation share a common ancestor. The observation that six Taiwanese families and a family from Chile both had this same mutation, but occurring on three different genetic backgrounds, suggests that the mutation p.P694L is both an ancestral and a recurrent mutation. The mutation p.P694L is the most frequent mutation underlying FPCA and is the only one that has been observed in two different ethnic groups. This may be partly explained by the sequence change (CCG > CTG) occurring at a CpG dinucleotide, a hotspot for mutagenesis.

By taking a positional candidate approach, two genes (*OSMR* and *IL31RA*) of the IL-6 cytokine pathway are now recognized to be associated with FPCA. It remains to be determined how the signaling changes induced by *OSMR* and *IL31RA* mutations led to the PCA phenotypes. Severe itching is a hallmark of PCA[19] and prolonged scratching might induce apoptosis and lead to PCA.[5] It has been shown that normal human epidermal keratinocyte cell lines expressed gp130, IL-31RA, and OSMRβ, and responded to OSM and IL-31 activation.[34–35] In skin, IL-31 induces severe pruritus and dermatitis in transgenic mice.[34] High IL-31 levels were detected in prurigo nodularis, one of the most pruritic forms of chronic skin inflammation.[36] Moreover, dorsal root ganglion expressed very high level of IL-31RA mRNA[36] and OSMRβ has been detected on a specific subset of

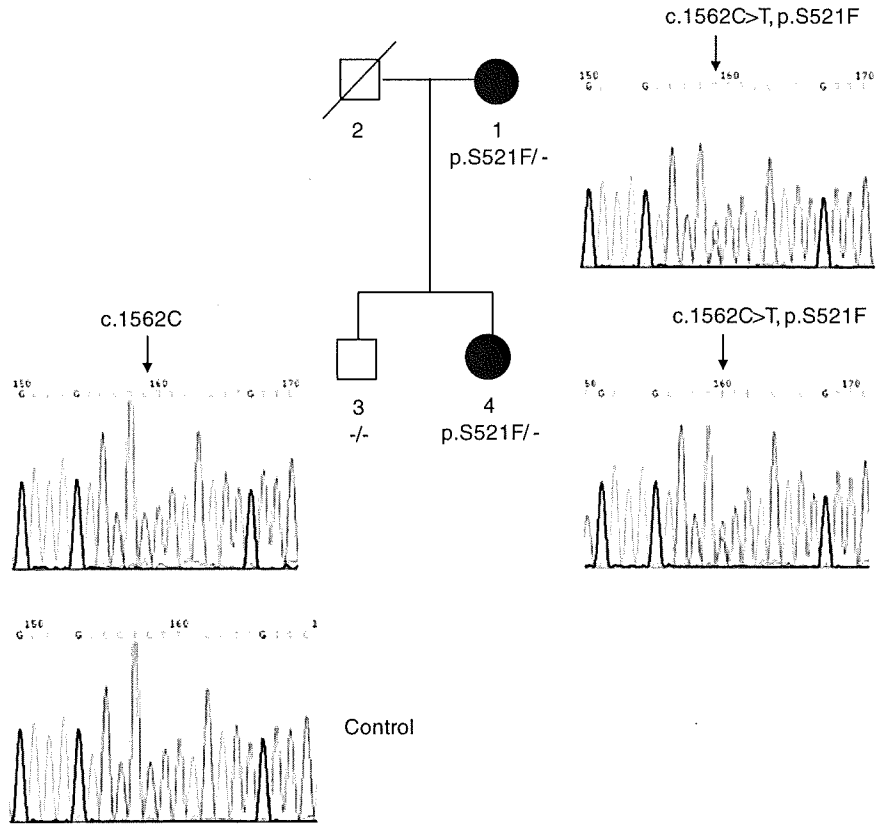

Figure 3 Genetic analysis of the *IL31RA* mutation p.S521F in a FPCA pedigree. Sequencing of the exon 12 of the *IL31RA* gene in Pedigree L revealed c.1562C>T (NM_139017) heterozygous transition in two affected individuals (#1 and #4) whereas unaffected individual (#3) did not harbor this variation.

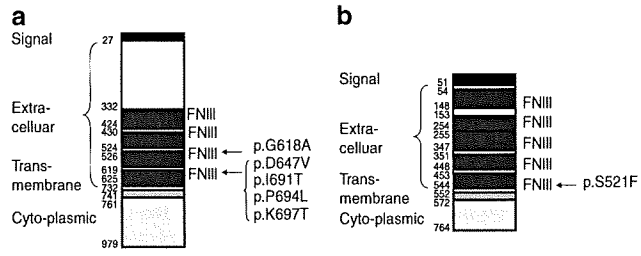

Figure 4 Diagrammatic representation of OSMRβ (**a**) and IL-31RA (**b**), showing the functional domains of the encoded proteins and the positions of mutated codons. Amino-acid numbers are shown to the left of the diagram and the sites of the missense mutations to the right. The p.G618A and p.I691T mutations were reported earlier by Arita *et al*. The figure of IL-31RA is based on the amino-acid sequence of isoform 2. FNIII, fibronectin type III-like domain. Adapted from http://www.uniprot.org/uniprot/Q99650 (OSMRβ) and http://www.expasy.org/uniprot/q8ni17 (IL-31RA).

nociceptive neurons in dorsal root ganglion,[37–38] suggesting that IL-31 might induce pruritus by directly modulating the function of sensory neurons.

The genetic heterogeneity for PCA presented by mutations in two physically adjacent and functionally related genes is intriguing. OSMRβ is a common component of both the OSM type II receptor and the IL-31 receptor. It will be of interest to dissect the signaling pathways mediated by the OSM and IL-31 receptors under different cultured conditions to investigate the molecular mechanism(s) leading to PCA pathogenesis. It is known that the two cytokine receptors mediate distinct signaling reactions and response patterns in lung epithelial cells.[39] IL-31 was significantly over-expressed in skin samples from patients with atopic dermatitis but not with psoriasis.[36] On the contrary, expression of both OSM type II receptor and OSM were enhanced in both psoriatic and atopic dermatitic lesions, two common inflammatory skin disorders.[35] Mainly secreted by activated T cells, monocytes, and dendritic cells, OSM is also a potent inducer of keratinocyte migration and triggers hyperplasia of the reconstituted human epidermis.[35] Although PCA itself is not considered as an inflammatory skin disease, further investigation of the OSMRβ-related signaling pathways might lead to better understanding of the pathogenesis and to the identification of new therapeutic targets for PCA.

In summary, the genetic data collected from this investigation clearly support multi-origins of *OSMR* mutations in different populations, and we conclude that haplotype comparison between PCA families in Taiwan, a region of high prevalence, offers a case for studying the evolution and dissemination of a mutant allele in this population. In view of cytokine-receptors-mediated signaling in the skin, our finding on the frequent *OSMR* mutations and the discovery of *IL31RA* mutation in PCA patients might shed light on future study of disease pathophysiology. New knowledge about the abnormal cellular signaling in PCA is a key to developing novel therapeutics for this relatively common skin disease for our patients.

ACKNOWLEDGEMENTS

We thank Dr Tsung-Sheng Su for critical reading of the manuscript, the patients, and members of the PCA families who participated in this study, Ms Li-Ru Chen, Ms Ying-Chen Chang, and Ms Ying-Yen Weng for excellent technical support, and the staff of the Department of Dermatology, Taipei Veterans General Hospital, for referral of PCA subjects. This work was supported in part by grants VGH 93-354, VGHUST94-P1-14,

NSC94-3112-B-010-019, NSC95-3112-B-010-001, NSC96-3112-B-010-001, NSC97-2314-B-010-016-MY2, and a grant from The Ministry of Education, Taiwan, Aim for the Top University Plan. The linkage analysis server was supported by grants VGH 94-368-2, V95S2-003, and V96S2-005. The sequencing services and Affymetrix 10K SNP assays were provided by the Sequencing Core Facility and Gene Expression Core Facility of the National Research Program for Genomic Medicine supported by grants from the National Science Council, Taiwan, respectively. Studies on PCA in the UK were kindly supported by a grant from Action Medical Research.

1 Wong CK: Lichen amyloidosus: a relatively common skin disorder in Taiwan. *Arch Dermatol* 1974; **110**: 438–440.
2 Ollague W, Ollague J, Ferretti H: Epidemiology of primary cutaneous amyloidoses in South America. *Clin Dermatol* 1990; **8**: 25–29.
3 Tan T: Epidemiology of primary cutaneous amyloidoses in Southeast Asia. *Clin Dermatol* 1990; **8**: 20–24.
4 Wong CK, Lin CS: Friction amyloidosis. *Int J Dermatol* 1988; **27**: 302–307.
5 Chang YT, Wong CK, Chow KC, Tsai CH: Apoptosis in primary cutaneous amyloidosis. *Br J Dermatol* 1999; **40**: 210–215.
6 Chang YT, Liu HN, Wong CK, Chow KC, Chen KY: Detection of Epstein-Barr virus in primary cutaneous amyloidosis. *Br J Dermatol* 1997; **136**: 823–826.
7 Porto JA, Posse FA: Amiloidose cutanea genuina familial. *Bol Da Soc Brasil Dermatol E Sif* 1960; **35**: 102–103.
8 de Souza AR: Amiloidose cutanea bohlosa familial. Observacao de 4 casos. *Rev Hosp Clin Fac Med S Paolo* 1963; **18**: 413–417.
9 Sagher F, Shanon J: Amyloidosis cutis. *Arch Dermatol* 1963; **87**: 171–175.
10 Tay CH: Genodermatoses in Singapore – a genetic study of certain skin diseases. *Asian J Med* 1971; **7**: 413–422.
11 Rajagopalan K, Tay CH: Familial lichen amyloidosis. Report of 19 cases in 4 generations of a Chinese family in Malaysia. *Br J Dermatol* 1972; **87**: 123–129.
12 Vasily DB, Bhatia SG, Uhlin SR: Familial primary cutaneous amyloidosis. *Arch Dermatol* 1978; **114**: 1173–1176.
13 de Pietro WP: Primary familial cutaneous amyloidosis. *Arch Dermatol* 1981; **117**: 639–642.
14 Ozaki M: Familial lichen amyloidosis. *Int J Dermatol* 1984; **23**: 190–193.
15 Newton JA, Jagjivan A, Bhogal B, McKee PH, McGibbon DH: Familial primary cutaneous amyloidosis. *Br J Dermatol* 1985; **112**: 201–208.
16 Lee DD, Huang JY, Wong CK, Gagel RF, Tsai SF: Genetic heterogeneity of familial primary cutaneous amyloidosis: lack of evidence for linkage with the chromosome 10 pericentromeric region in Chinese families. *J Invest Dermatol* 1996; **107**: 30–33.
17 Bergamo F, Annessi G, Ribuffo M: Familial lichen amyloidosis. *Chron Dermatol* 1997; **6**: 959–961.
18 Hartshorne ST: Familial primary cutaneous amyloidosis in a South African family. *Clin Exp Dermatol* 1999; **24**: 438–442.
19 Wang WJ, Chang YT, Huang CY, Lee DD: Clinical and histopathological characteristics of primary cutaneous amyloidosis in 794 Chinese patients. *Zhonghua Yi Xue Za Zhi (Taipei)* 2001; **64**: 101–107.
20 Lin MW, Lee DD, Lin CH *et al*: Suggestive linkage of familial primary cutaneous amyloidosis to a locus on chromosome 1q23. *Br J Dermatol* 2005; **152**: 29–36.
21 Lee DD, Lin MW, Chen IC *et al*: Genome-wide scan identifies a susceptibility locus for familial primary cutaneous amyloidosis on chromosome 5p13.1-q11.2. *Br J Dermatol* 2006; **155**: 1201–1208.
22 Arita K, South AP, Hans-Filho G *et al*: Oncostatin M receptor-β mutations underlie familial primary localized cutaneous amyloidosis. *Am J Hum Genet* 2008; **82**: 73–80.
23 Scheller J, Ohnesorge N, Rose-John S: Interleukin-6 trans-signalling in chronic inflammation and cancer. *Scand J Immunol* 2006; **63**: 321–329.
24 Heinrich PC, Behrmann I, Haan S, Hermanns HM, Muller-Newen G, Schaper F: Principles of interleukin (IL)-6-type cytokine signalling and its regulation. *Biochem J* 2003; **374**: 1–20.
25 Stephens M, Sloan JS, Robertson PD, Scheet P, Nickerson DA: Automating sequence-based detection and genotyping of SNPs from diploid samples. *Nat Genet* 2006; **38**: 375–381.
26 The International HapMap Consortium: The International HapMap Project. *Nature* 2003; **426**: 789–796.
27 Lathrop GM, Lalouel JM, Julier C, Ott J: Multilocus linkage analysis in humans: detection of linkage and estimation of recombination. *Am J Hum Genet* 1985; **37**: 482–498.
28 Kruglyak L, Daly MJ, Reeve-Daly MP, Lander ES: Parametric and nonparametric linkage analysis: unified multipoint approach. *Am J Hum Genet* 1996; **58**: 1347–1363.
29 Barrett JC, Fry B, Maller J, Daly MJ: Haploview: analysis and visualization of LD and haplotype maps. *Bioinformatics* 2005; **21**: 263–265.
30 Zhao JH, Lissarrague S, Essioux L, Sham PC: GENECOUNTING: haplotype analysis with missing genotypes. *Bioinformatics* 2002; **18**: 1694–1695.
31 Zhao JH: 2LD, GENECOUNTING and HAP: computer programs for linkage disequilibrium analysis. *Bioinformatics* 2004; **20**: 1325–1326.
32 Kurth I, Horsten U, Pflanz S *et al*: Importance of the membrane-proximal extracellular domains for activation of the signal transducer glycoprotein 130. *J Immunol* 2000; **164**: 273–282.
33 Timmermann A, Küster A, Kurth I, Heinrich PC, Müller-Newen G: A functional role of the membrane-proximal extracellular domains of the signal transducer gp130 in heterodimerization with the leukemia inhibitory factor receptor. *Eur J Biochem* 2002; **269**: 2716–2726.
34 Dillon SR, Sprecher C, Hammond A *et al*: Interleukin 31, a cytokine produced by activated T cells, induces dermatitis in mice. *Nat Immunol* 2004; **5**: 752–760.
35 Boniface K, Diveu C, Morel F *et al*: Oncostatin M secreted by skin infiltrating T lymphocytes is a potent keratinocyte activator involved in skin inflammation. *J Immunol* 2007; **178**: 4615–4622.
36 Sonkoly E, Muller A, Lauerma AI *et al*: IL-31: a new link between T cells and pruritus in atopic skin inflammation. *J Allergy Clin Immunol* 2006; **117**: 411–417.
37 Morikawa Y, Tamura S, Minehata K-i, Donovan PJ, Miyajima A, Senba E: Essential function of oncostatin M in nociceptive neurons of dorsal root ganglia. *J Neurosci* 2004; **24**: 1941–1947.
38 Tamura S, Morikawa Y, Miyajima A, Senba E: Expression of oncostatin M receptor in a specific subset of nociceptive sensory neurons. *Eur J Neurosci* 2003; **617**: 2287–2298.
39 Chattopadhyay S, Tracy E, Liang P, Robledo O, Rose-John S, Baumann H: Interleukin-31 and oncostatin-M mediate distinct signaling reactions and response patterns in lung epithelial cells. *J Biol Chem* 2007; **282**: 3014–3026.

Supplementary Information accompanies the paper on European Journal of Human Genetics website (http://www.nature.com/ejhg)

6. Mohanty SK, Arora R, Kakkar N, Kumar B. Clear cell papulosis of the skin. *Ann Diagn Pathol.* 2002;6(6):385-388.
7. Kumarasinghe SP, Chin GY, Kumarasinghe MP. Clear cell papulosis of the skin: a case report from singapore. *Arch Pathol Lab Med.* 2004;128(11): e149-e152.
8. Chong WS, Ong BH, Kumarasinghe SP. Hypopigmented papules in an Asian boy. *Pediatr Dermatol.* 2005;22(3):268-269.
9. Benouni S, Kos L, Ruggeri SY, North PE, Drolet BA. Clear cell papulosis in Hispanic siblings. *Arch Dermatol.* 2007;143(3):358-360.
10. Toker C. Clear cells of the nipple epidermis. *Cancer.* 1970;25(3):601-610.
11. Slamon DJ, Clark GM, Wong SG, Levin WJ, Ullrich A, McGuire WL. Human breast cancer: correlation to relapse and survival with amplification of the HER2/neu oncogene. *Science.* 1987;235(4785):177-182.
12. Di Tommaso L, Franchi G, Destro A, et al. Toker cells of the breast: morphological and immunohistochemical characterization of 40 cases. *Hum Pathol.* 2008;39(9):1295-1300.

Bloody Nipple Discharge in an Infant

Bloody nipple discharge (BND) is occasionally observed in women with mammary disorders such as mastitis, intraductal papilloma, or breast carcinoma. However, this phenomenon is rarely seen in infants and children; BND in infants has seldom been reported in the dermatologic literature.

Report of a Case. A 4-month-old girl was referred to our clinic with a 1-week history of unilateral BND. Her mother reported a spontaneous and intermittent BND from the infant's left breast and denied breast manipulation or trauma. The infant was healthy except for BND and had no history of taking medication. The mother had no history of drug ingestion during either pregnancy or breastfeeding.

Physical examination of the chest and nipples showed no remarkable findings such as erythema, heat, tenderness, palpable mass, or enlargement of tissue. Pressure on the areolar area resulted in a bloody discharge from the left nipple (**Figure**, A). Ultrasonography of the left breast demonstrated dilatation of the retroareolar mammary ducts (Figure, B). The results of a blood cell count and coagulation tests were within the normal range. Culture of the bloody discharge revealed no bacterial growth. Cytologic examination of the secretion showed abundant erythrocytes but no other atypical cells. Based on these findings, bacterial infection and breast carcinoma were ruled out as a cause of the BND, and we decided to observe her without any treatment.

Comment. Bloody nipple discharge in infants, first described by Berkowitz and Inkelis,[1] occurs unilaterally or bilaterally in both sexes. Most patients older than 1 year show a palpable mass or breast enlargement, whereas infantile patients sometimes present with a normal appearance.[2] In laboratory examinations, coagulation test results and serum hormone levels are usually found to be normal, and culture of the discharge is usually negative.[2]

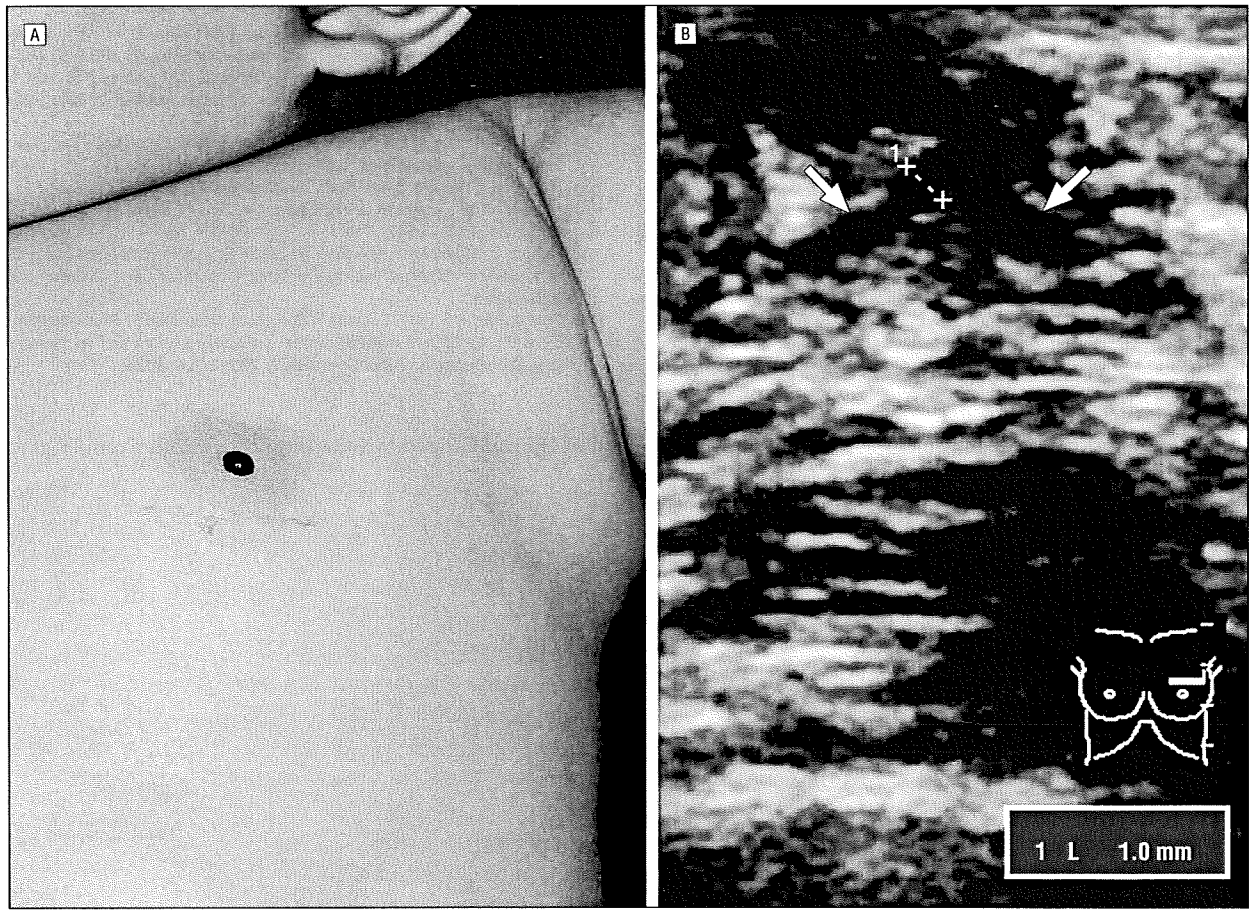

Figure. Bloody nipple discharge. A, Clinical appearance of bloody nipple discharge from the left breast. B, Ultrasonographic image of the left breast showing dilatation of the subareolar mammary ducts (arrows).

Histopathologically, mammary duct ectasia, a benign lesion characterized by dilated ducts surrounded by fibrosis and inflammation, has been proven in more than half of childhood BND cases with palpable masses treated surgically.[2] Mammary duct ectasia has also been detected by ultrasonography even in infantile cases with nonpalpable masses.[3,4] Underlying breast carcinoma should definitely be ruled out when we see patients with BND, but to our knowledge, it has never been reported in infants.[4,5] From these data, mammary duct ectasia is the most likely cause of BND in infants and children, although the specific cause of duct ectasia remains unclear.

To our knowledge, all but 1 of the reported BND cases in infants has achieved spontaneous resolution within 9 months.[3-5] The 1 case that did not resolve spontaneously was treated surgically. These facts suggest that BND in infants is a benign and self-limiting condition. Therefore, invasive intervention, including biopsy, should be avoided, especially in girls, because even minimal operative injury to the breast bud may produce severe tissue damage resulting in functional disability and persistent disfigurement.[4,5] Noninvasive investigations such as culture of the discharge and ultrasonographic evaluation are recommended as well as a careful physical examination and close clinical follow-up. Only if ultrasonography reveals a mass or abnormality other than mammary duct ectasia, or if the discharge persists for more than 9 months, should further investigations, including invasive interventions, be considered.[5]

Hideyuki Ujiie, MD
Masashi Akiyama, MD, PhD
Rinko Osawa, MD
Satoru Shida, MD, PhD
Satoru Aoyagi, MD, PhD
Hiroshi Shimizu, MD, PhD

Correspondence: Dr Ujiie, Department of Dermatology, Hokkaido University Graduate School of Medicine, North 15 W 7, Kita-ku, Sapporo 060-8638, Japan (h-ujiie@med.hokudai.ac.jp).
Financial Disclosure: None reported.

1. Berkowitz CD, Inkelis SH. Bloody nipple discharge in infancy. *J Pediatr*. 1983; 103(5):755-756.
2. Imamoglu M, Cay A, Reis A, Ozdemir O, Sapan L, Sarihan H. Bloody nipple discharge in children: possible etiologies and selection of appropriate therapy. *Pediatr Surg Int*. 2006;22(2):158-163.
3. Weimann E. Clinical management of nipple discharge in neonates and children. *J Paediatr Child Health*. 2003;39(2):155-156.
4. De Praeter C, De Coen K, Vanneste K, Vanhaesebrouck P. Unilateral bloody nipple discharge in a two-month-old male. *Eur J Pediatr*. 2008;167(4):457-459.
5. Kelly VM, Arif K, Ralston S, Greger N, Scott S. Bloody nipple discharge in an infant and a proposed diagnostic approach. *Pediatrics*. 2006;117(4):e814-e816.

Acute Generalized Exanthematous Pustulosis Caused by Rifabutin

Acute generalized exanthematous pustulosis (AGEP), first named by Beylot et al[1] in 1980, is a clinical reaction pattern that is principally drug induced.[2,3] Its incidence is probably underestimated because many cases are either unrecognized or confused with pustular psoriasis.[3] We report herein a case of AGEP caused by rifabutin, an antituberculous agent.

Report of a Case. A 58-year-old man with hypertension, coronary artery disease, and schizophrenia was admitted to our hospital for cervical nontuberculous mycobacterial lymphadenitis. He had a history of drug allergy to trimethoprim-sulfamethoxazole presenting as a generalized nonpustular exanthematous eruption. After 10 days of treatment with rifabutin, he developed a fever with temperatures up to 38°C accompanied by numerous nonfollicular sterile pustules on widespread edematous erythema over the trunk and all extremities without mucous membrane involvement (**Figure 1**).

Laboratory examinations revealed leukocytosis with left shift and mild eosinophilia. (The white blood cell count was 11200/μL; neutrophil-bands, 12%; eosinophil-bands, 7%; to convert white blood cells to 10^9/L, multiply by 0.001.) Histopathologic evaluation showed spongiform subcorneal pustules with a predominance of neutrophils and eosinophils and papillary dermal edema with perivascular inflammatory cell infiltrate (**Figure 2**).

Rifabutin treatment was discontinued, and intravenous hydrocortisone, 100 mg, was administered every 6 hours. The pustules resolved rapidly with generalized desquamation and have not recurred. Acute generalized exanthematous pustulosis was confirmed by validation score of the EuroSCAR study group.[2]

Comment. More than 90% of AGEP cases are drug induced, mainly by antibiotics, especially ß-lactams and macrolides.[2,3] Our patient had no personal or family his-

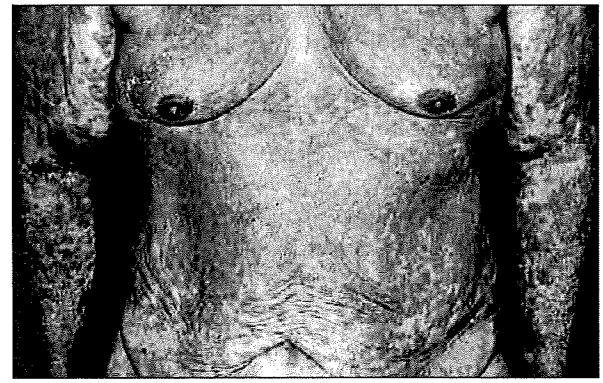

Figure 1. Numerous nonfollicular pinhead sterile pustules on edematous and erythematous plaques over trunk and all extremities.

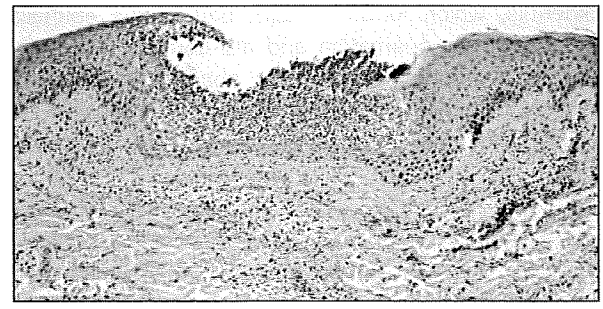

Figure 2. Spongiform subcorneal pustule with mixed neutrophils and eosinophils and a focal necrosis of keratinocytes in the epidermis (hematoxylin-eosin, original magnification ×100).

Glycosylation Specific for Adhesion Molecules in Epidermis and Its Receptor Revealed by Glycoform-focused Reverse Genomics*[S]

Rie Uematsu‡, Yasuro Shinohara‡§, Hiroaki Nakagawa‡, Masaki Kurogochi‡, Jun-ichi Furukawa‡, Yoshiaki Miura‡, Masashi Akiyama¶, Hiroshi Shimizu¶, and Shin-Ichiro Nishimura‡‖

Glycosylation of proteins greatly affects their structure and function, but traditional genomics and transcriptomics are not able to precisely capture tissue- or species-specific glycosylation patterns. We describe here a novel approach to link different "omics" data based on exhaustive quantitative glycomics of murine dermis and epidermis. We first examined the dermal and epidermal *N*-glycome of mouse by a recently established glycoblotting technique. We found that the Galα1–3Gal epitope was solely expressed in epidermis tissue and was preferentially attached to adhesion molecules in a glycosylation site-specific manner. Clarified glycomic and protemic information combined with publicly available microarray data sets allowed us to identify galectin-3 as a receptor of Galα1–3Gal epitope. These findings provide mechanistic insight into the causal connection between the genotype and the phenotype seen in α3GalT-1-deficient mice and transgenic mice expressing endo-β-galactosidase C. Because humans do not possess the Galα1–3Gal structure on their tissues, we further examined the human dermal and epidermal *N*-glycome. Comparative glycomics revealed that the GalNAcβ1–4GlcNAc (*N,N'*-diacetyllactosediamine) epitope, instead of the Galα1–3Gal epitope, was highly expressed in human epidermis. ***Molecular & Cellular Proteomics 8:232–244, 2009.***

Posttranslational protein glycosylation changes the biological and physical properties of glycoconjugates, which include functions as signals or ligands to control their distribution, antigenicity, metabolic fate, stability, and solubility (1). Cells in the epidermis, which forms a major part of the epithelial barrier, undergo desquamation and are continuously being renewed (2), a process that requires changes in adhesion. Because glycoproteins are often involved in adhesion between cells and their extracellular matrices, the glycoproteome of the epidermis may therefore provide new insight into the functional roles of protein glycosylation. Mammalian epidermal glycoconjugates have mostly been studied histochemically using lectins (3) or monoclonal antibodies (4). Although these studies revealed that the cell surfaces of keratinocytes in the epidermis contain numerous glycoconjugates, these approaches cannot provide detailed structural information about the oligosaccharides or their carrier proteins.

We previously clarified the quantitative glycomic profile of murine dermis and epidermis using novel aminooxy-based isotope tags and MALDI-TOF MS analysis (5), which revealed distinct features of the *N*-glycosylation profile of dermis and epidermis. We found that murine epidermal glycoproteins have a high abundance of high mannose-type oligosaccharides, and the striking roles of lysosomal enzymes in epidermis during lipid remodeling and desquamation were further discussed. This study was the first to demonstrate the usefulness of quantitative gross *N*-glycan profiling for performing systematic glycoform-focused proteomics. To advance and accelerate this approach, we recently established a novel technology platform for large scale quantitative glycomics based on the glycoblotting technique (6–8). In this method, glycans derived from biological samples are selectively captured onto novel high density hydrazide beads (BlotGlyco H) for highly efficient purification of oligosaccharides from complex biological samples. The captured oligosaccharides are subjected to on-bead methyl esterification to stabilize sialic acid(s) for the simultaneous quantitation of neutral and sialylated oligosaccharides by MALDI-TOF MS and are finally recovered as arbitrary derivatives by imine exchange chemistry.

In the current study, we first used this newly established glycoblotting technique to re-examine both the neutral and sialylated *N*-glycome of murine dermis and epidermis. We detected 75 oligosaccharides, more than twice the amount detected previously when sialic acids were removed, thus enabling us to perform a more detailed comparison of tissue-specific *N*-glycosylation profiles. We found that the expression of oligosaccharides containing the Galα1–3Gal epitope was only detected in epidermis, although many non-reducing terminal epitopes tend to vanish in epidermis. Tracing from

From the ‡Graduate School of Advanced Life Science, Hokkaido University, Sapporo 001-0021, Japan and ¶Department of Dermatology, Hokkaido University Graduate School of Medicine, Sapporo 060-8638 Japan

Received, April 1, 2008, and in revised form, August 29, 2008
Published, MCP Papers in Press, September 29, 2008, DOI 10.1074/mcp.M800145-MCP200

the glycome back to the proteome and transcriptome allowed us to identify a group of proteins that carry Galα1–3Gal epitope and a receptor that can recognize Galα1–3Gal epitope. The glycans identified in mice epidermis could account for the phenotypes observed in transgenic mice expressing endo-β-galactosidase C. Finally human epidermal glycomics was evaluated aiming to address the question of whether any alternative glycan structures play a role similar to that of the Galα1–3Gal epitope in murine epidermis.

EXPERIMENTAL PROCEDURES

Skin Samples and Tissue Preparation—Male hairless mice (Hos/HR-1) were obtained from Sankyo Labo Service (Tokyo, Japan). They were fed a standard mouse diet and water *ad libitum*. Full thickness skin samples were taken from the dorsal area of 7–12-week-old animals. Animal experiments were performed according to the respective regulatory standards of Hokkaido University. Normal human skin samples were obtained from patients during resection operations. The medical ethics committee at Hokkaido University approved all of the described studies, and all of the participants gave their written informed consent. After removal of excess subcutaneous fat from the skin samples, the epidermis was peeled from the dermis by heat separation at 60 °C for 30 s. The epidermis and dermis were minced and heated at 90 °C for 10 min in 10 mM ammonium bicarbonate, then defatted as described by Bligh and Dyer (9), and lyophilized.

N-Glycan Release—*N*-Glycans were released from tissues in previously optimized conditions (10) with minor modifications. Each defatted and lyophilized tissue (equivalent to 3 mg) was suspended in 0.02% 1-propanesulfonic acid, 2-hydroxy-3-lauramido in 10 mM ammonium bicarbonate; reduced with DTT; *S*-carbamoylmethylated; and digested with trypsin (Sigma). Following deglycosylation by treatment with peptide-*N*-glycosidase F (PNGase F;[1] Hoffmann-La Roche), the samples were digested with Pronase (Calbiochem). The supernatant was evaporated to dryness and redissolved in 120 μl of 10 mM ammonium bicarbonate.

N-Glycan Purification and Derivatization—*N*-Glycans in the de-*N*-glycosylated sample were purified and labeled by using a previously described method (7). Briefly 20-μl aliquots of epidermis and dermis samples were applied to a polymer displaying hydrazide functionality at high density (BlotGlyco H), 180 μl of 2% acetic acid in acetonitrile was added, and the released *N*-glycans were captured via hydrazone linkage by incubation at 80 °C for 45 min. After the beads were washed with 2 M guanidine hydrochloride in ammonium bicarbonate, H_2O, and 1% triethylamine in methanol, 10% acetic anhydride in methanol was added, and the solution was incubated at room temperature for 30 min to cap the residual hydrazide groups. Following the washing of the beads with 10 mM hydrochloric acid, methanol, and dioxane, the sialic acids were methyl esterified by incubation at 60 °C for 60 min with 100 mM 3-methy-1-*p*-tolyltriazene in dioxane. The beads were washed with dioxane, H_2O, methanol, and H_2O, and then 20 μl of 20 mM N^{α}-((aminooxy)acetyl)tryptophanylarginine methyl ester (aoWR) and 180 μl of 2% acetic acid in acetonitrile were added. The solutions were heated at 80 °C for 45 min to transfer the glycans captured on the beads to aoWR, and the glycans were eluted with H_2O. To remove the excess aoWR, an aliquot of each sample was applied to a MassPREP™ hydrophilic interaction chromatography μElution Plate (Waters, Milford, MA) according to the manufacturer's instructions with minor modifications. Following washing with 1% acetic acid, the wells were equilibrated with 1% acetic acid in 95% acetonitrile. After the addition of each sample, the wells were washed with equilibration solution and eluted with 1% acetic acid in 5% acetonitrile.

N-Glycan Profiling by MALDI-TOF—Each purified aoWR-derivatized sample was dried and diluted with 10 μl of 2,5-dihydroxybenzoic acid (DHB; 10 mg/ml in 30% acetonitrile; Bruker Daltonics, Bremen, Germany), and an aliquot (1 μl) was deposited on the stainless steel target plate. The aoWR derivatized samples were analyzed to elucidate the relative quantities of the different oligosaccharides present in each tissue. MALDI-TOF data were obtained using an Ultraflex time-of-flight mass spectrometer (Bruker Daltonics) equipped with a LIFT-TOF/TOF unit controlled by the FlexControl 2.2 software package. All of the spectra were obtained using the reflectron mode with an acceleration voltage of 25 kV, a reflector voltage of 26.3 kV, and a pulsed ion extraction of 160 ns in the positive ion mode. The results were obtained by accumulating the signals of 1,000 laser shots. The signal intensity of each mass was automatically calculated by FlexAnalysis 2.0. Estimations of *N*-linked type oligosaccharide structures were obtained by entering the peak masses into the GlycoMod Tool (Swiss Institute of Bioinformatics) and GlycoSuite (Proteome Systems).

Neutral N-Glycan Profiling by the Two-dimensional Mapping Technique—Each sample was also analyzed by derivatization with 2-aminopyridine (PA) followed by the two-dimensional mapping technique as described previously (11, 12). Briefly *N*-glycans in the de-*N*-glycosylated sample were purified by gel filtration and derivatized with PA and sodium cyanoborohydride. After removal of unreacted PA by Sephadex G-15 (GE Healthcare), the PA-oligosaccharides were further purified by collecting the elution from amide-80 (4.6 × 250 mm, Tosoh, Tokyo, Japan) using HPLC. The mixture of PA-oligosaccharides was applied to an octadecylsilyl silica (ODS; 6 × 150 mm, Shimadzu, Kyoto, Japan) HPLC column, and the elution times of the individual peaks were normalized with reference to the PA-derivatized isomalto-oligosaccharides of polymerization degree 4–20 and represented by GU (ODS). Then individual fractions separated on the ODS column were applied to the amide-80 column. Similarly the retention time of the individual peaks on the amide-80 column were represented by GU (amide). Thus, a given compound from these two columns provided a set of GU (ODS) and GU (amide) values, which corresponded to coordinates of the two-dimensional sugar map. By comparison with the coordinates of reference PA-oligosaccharides, the *N*-glycans from skin were identified. Identification was confirmed by co-chromatography with a candidate reference on the columns and sequential exoglycosidase digestion. Molar ratios of *N*-glycans were calculated from the individual peak areas.

MALDI-TOF/TOF MS of PA-derivatized N-Glycans Using the Matrix-dependent Selective Fragmentation (MDSF) Method—Some of the PA-derivatized *N*-glycans also were analyzed by MALDI-LIFT-TOF/TOF MS using MDSF according to the procedure described previously (13, 14). α-Cyano-4-hydroxycinnamic acid (Bruker Daltonics) was prepared as a saturated solution in 3:1 (v/v) acetonitrile/water. The desalted PA-derivatized *N*-glycan samples were dissolved in water, applied on the target spot of the stainless steel target plate, mixed with 1 μl of matrix solution (either 2,5-dihydroxybenzoic acid or

[1] The abbreviations used are: PNGase F, peptide-*N*-glycosidase F; ConA, concanavalin A; aoWR, N^{α}-((aminooxy)acetyl)tryptophanylarginine methyl ester; LacdiNAc, *N,N'*-diacetyllactosediamine (GalNAcβ1–4GlcNAc); PA, 2-aminopyridine; ODS, octadecylsilyl silica; MDSF, matrix-dependent selective fragmentation; Ah, anthraniloyl hydrazine; SPR, surface plasmon resonance; Fuc, fucose; M2, $Man_2GlcNAc_2$; M3, $Man_3GlcNAc_2$; M3F, $Man_3GlcNAc_2Fuc$; M4, $Man_4GlcNAc_2$; NeuAc, *N*-acetylneuraminic acid; NeuGc, *N*-glycolylneuraminic acid; MHC, major histocompatibility complex; Susd 2, sushi domain-containing protein-2; α3GalT, α1,3-galactosyltransferase; GU, glucose unit.

α-cyano-4-hydroxycinnamic acid), and dried at room temperature. All measurements were performed using an Ultraflex TOF/TOF mass spectrometer equipped with a reflector and controlled by the FlexControl 2.2 software package (Bruker Daltonics). In MALDI-TOF MS reflector mode, ions generated by a pulsed UV laser beam (nitrogen laser, λ = 337 nm, 5 Hz) were accelerated to a kinetic energy of 23.5 kV. Metastable ions generated by laser-induced decomposition of the selected precursor ions were analyzed without any additional collision gas. In MALDI-LIFT-TOF/TOF mode, precursor ions were accelerated to 8 kV and selected in a timed ion gate. The fragments were further accelerated by 19 kV in the LIFT cell, and their masses were analyzed after the ion reflector passage. Masses were automatically annotated by using the FlexAnalysis 2.2 software package.

Preparation of Glycopeptides—Defatted and lyophilized murine epidermis (30–50 mg) was dissolved in a solution of 7 M guanidine hydrochloride, 0.5 M Tris-HCl, pH 8.5, and 10 mM EDTA; reduced with DTT; and *S*-carbamidomethylated. The alkylated proteins were dialyzed against 10 mM ammonium bicarbonate and digested with trypsin. The digested proteins were applied to a concanavalin A (ConA)-agarose (Seikagaku Co., Tokyo, Japan) column equilibrated with a solution of 150 mM NaCl, 1 mM $MgCl_2$, 1 mM $CaCl_2$, and 10 mM Tris-HCl buffer, pH 7.5. After the column was washed with equilibrated buffer, the glycopeptides carrying biantennary complex-type oligosaccharides were eluted with buffer containing 10 mM methyl α-glucopyranoside. The eluted glycopeptides were then separated on an ODS column using HPLC with a linear gradient of acetonitrile (0–32%) in 0.1% formic acid. Chromatography was carried out at a flow rate of 1 ml/min at room temperature and was monitored at 214 nm. The glycopeptide mixture was separated into 100 fractions and dried with a centrifugal vacuum concentrator. The fractionated glycopeptides were dissolved in 10 μl of 30% acetonitrile. A portion (1 μl) of each fraction was deglycosylated by PNGase F and dissolved in the matrix solution.

Glycopeptide Identification by MALDI-TOF/TOF—Each fraction with and without PNGase F treatment was mixed with 2,5-dihydroxybenzoic acid (10 mg/ml in 30% acetonitrile) and then applied to the MALDI target plate. MALDI-TOF and MALDI-TOF/TOF data were obtained using an Ultraflex time-of-flight mass spectrometer as above. For fragmentation ion analysis in the TOF/TOF mode, precursors were accelerated to 8 kV and selected in a timed ion gate. Fragment ions generated by laser-induced decomposition of the precursor were further accelerated by 19 kV in the LIFT cell, and their masses were analyzed after passing the ion reflector. Masses were automatically annotated by using FlexAnalysis 2.0. External calibration of MALDI-TOF MS was carried out using singly charged monoisotopic peaks and fragments of a mixture of human angiotensin II (*m/z* 1046.542; Bruker Daltonics), bombesin (*m/z* 1619.823; Bruker Daltonics), and adrenocorticotropic hormone-(18–39) (*m/z* 2465.199; Bruker Daltonics).

Protein Identification by Database Search—Peak lists were generated from the MS/MS spectra using Bruker FlexAnalysis (Version 2.0) and were processed by the MASCOT™ (Version 2.1, Matrix Science, London, UK) search algorithm to assign peptides based on the Mass Spectrometry Protein Sequence Database (MSDB database updated February 27, 2005, 1,942,918 sequences), a database containing 75,031 mouse genome sequences. The database was searched for tryptic peptides with up to one miscleavage and a mass tolerance for the precursor ions of 1.2 Da and for the fragment ions of 2.0 Da. All cysteine residues were treated as being carbamidomethylated. Deamidation of asparagines caused by deglycosylation was considered. We first screened the candidate peptides with probability-based MOWSE (molecular weight search) scores that exceeded their thresholds ($p < 0.05$) and with MS/MS signals for y- or b-ions >5. If the peptide did not contain the consensus tripeptide sequence for *N*-linked glycosylation (N*X*(S/T)) the data were eliminated regardless of the matching score. In total, 14 sets of MS/MS data were obtained.

Determination of the Relative Quantities of the Microheterogeneous Glycoforms Present at Each N-Glycan Binding Site—Following the fractionation of ConA-bound fractions (eluted with buffer containing 10 mM methyl α-glucopyranoside or 100 mM methyl α-mannopyranoside), each fraction was further analyzed by reversed-phase chromatography as described previously (5). The relative quantitation of the microheterogeneity of different glycoforms present at a particular *N*-glycan binding site was determined by comparing the signal intensities upon mixing the same volume from each successive fraction that contained the same peptide backbone.

Purification of Oligosaccharide Having Galα1–3Gal Epitope and Labeling with Biotin—Purification of oligosaccharide having the Galα1–3Gal epitope and its labeling with biotin were performed as described previously (7). Briefly alkylated and dialyzed murine epidermal proteins were digested with trypsin/PNGase F and were subjected to glycoblotting as described above. The blotted oligosaccharides were recovered as anthraniloyl hydrazine (Ah) derivatives, which are fluorogenic and suitable for chromatographic separation. Ah-derivatized oligosaccharides were subjected to ConA immobilized affinity chromatography and normal-phase HPLC according to the procedure described previously (15). Purified oligosaccharides (100 pmol) were dissolved in 2% acetic acid in 98% acetonitrile and were incubated with aminooxy biotin (Biotium, Inc.) (2 nmol) to promote the conversion of Ah derivatives to biotin derivatives. To remove the excess aminooxy biotin, an aliquot of samples was applied to an amide-80 column.

Surface Plasmon Resonance Analysis—The aminooxy-labeled oligosaccharide (10 pmol) was introduced onto a streptavidin preimmobilized sensor surface (sensor chip SA-5 (BIACORE AB, Uppsala, Sweden)). Recombinant murine galectin-3 and -7 (R&D Systems, Inc.) were purified with Superdex 200 10/300 GL (GE Healthcare) to remove excess carrier protein. Interactions were monitored by surface plasmon resonance (SPR) using a BIACORE 2000 system (BIACORE AB) as described previously (16). The reference flow cell sensorgram (determined by injection over a blank surface) was subtracted from the corresponding sensorgrams to abolish base-line drift, bulk, and nonspecific interaction contributions.

RESULTS AND DISCUSSION

Gross N-Glycan Profiling of Murine Dermis and Epidermis—We analyzed the murine dermal and epidermal *N*-glycomes using a recently established glycoblotting technique (7) that utilizes a polymer displaying high density hydrazide functionality (BlotGlyco H) coupled with solid-phase methyl esterification of sialic acids and subsequent tag conversion by aoWR, a labeling reagent (MS probe) for highly sensitive MALDI-TOF MS. As shown in Fig. 1, the MALDI-TOF MS spectra obtained from each sample differed substantially; the epidermal glycome tended to be of smaller molecular size than dermal glycome. We detected 75 oligosaccharides in either dermis or epidermis, more than twice the number detected previously when sialic acids were removed (5). This great increase is attributable not only to the addition of a variety of sialylated species but also to improved detection sensitivity from the drastically improved signal-to-noise ratio obtained with the glycoblotting technique because of its extremely high purification power. The structure and relative abundance of each detected oligosaccharide are summarized

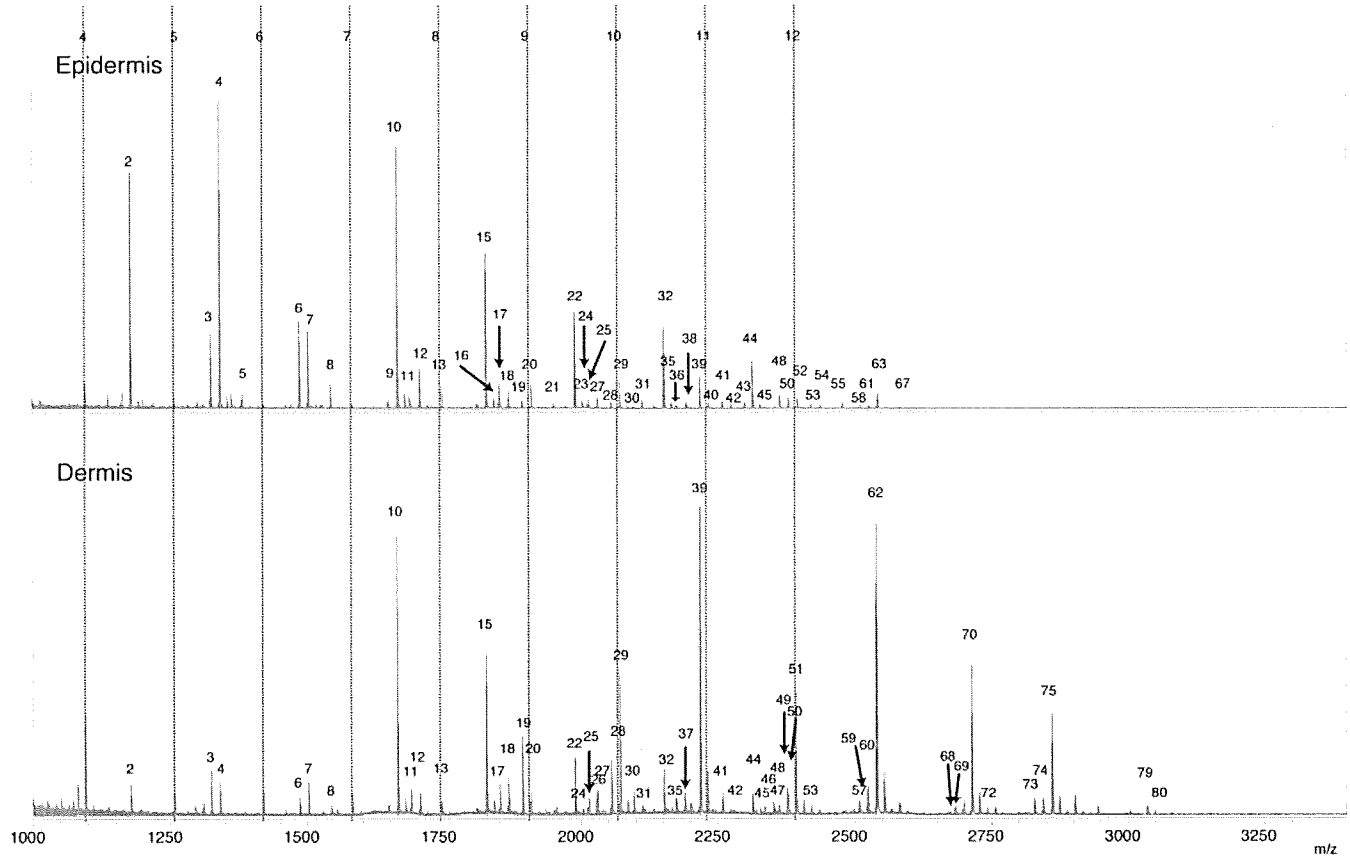

FIG. 1. **MALDI-TOF spectra showing the *N*-glycan profiles of murine skin glycoproteins.** *N*-Glycans derived from skin tissues were derivatized with aoWR(H). The putative compositions of the *numbered* oligosaccharide signals are shown in Table I. *Dotted lines* with *numbers* were putatively assigned to be hexose oligomers ($(Hex)_{4-12}$).

in Table I. We quantified the relative abundance of each type of structure in the observed oligosaccharides (Fig. 2). High mannose-type oligosaccharides, including $Man_2GlcNAc_2$ (M2), $Man_3GlcNAc_2$ (M3), $Man_3GlcNAc_2Fuc$ (M3F), and $Man_4GlcNAc_2$ (M4) were more highly expressed in epidermis than in dermis (Fig. 2*a*). The relative abundance of M2, M3, M3F, and M4, which are considered to be degraded products according to the well characterized *N*-glycan biosynthesis (17), was much higher in epidermis than in dermis (Fig. 2*b*, "*Others*") in good agreement with our previous report (5).

Sialylated species were scarcely observed in epidermis, whereas ~40% of dermal *N*-glycans were found to be sialylated (Fig. 2*a*). In mice, the sialylated species include both *N*-acetylneuraminic acid (NeuAc) and *N*-glycolylneuraminic acid (NeuGc), but NeuGc was the major sialic acid form (Fig. 2*c*). The relative abundance of oligosaccharides having one or more fucose residues was also substantially lower in epidermis than in dermis; fewer than 30% of epidermal oligosaccharides were modified with fucose, whereas 50–60% of dermal oligosaccharides were fucosylated (Fig. 2*d*). The relatively smaller molecular size observed for the epidermal *N*-glycome may in part be attributable to decreased sialylation as well as fucosylation. This finding, in conjunction with the marked increase of M2, M3, M4, and their fucosylated analogues in epidermis, suggests that glycoforms of epidermal glycoproteins are often trimmed by several glycosidases. These observations most likely reflect the unique epidermal environment, which is rich in degradation enzymes, including various glycosidases, because of the desquamation of living cells (18). Thus although many non-reducing terminal epitopes vanished, interestingly the expression of oligosaccharides containing the Galα1–3Gal epitope was only detected in epidermis (Fig. 2*e*). The presence of the Galα1–3Gal epitope in mice epidermis was predicted from the histochemical studies using *Griffonia simplicifolia*-I (GS-I), a lectin known to bind to the Galα1–3Gal epitope (19), although the histochemical approach does not clarify whether the glycoconjugate of interest is a glycolipid or an *N*-glycosylated or *O*-glycosylated glycoprotein.

Reverse Proteomics/Genomics of the Galα1–3Gal Epitope—The unique expression profile of Galα1–3Gal in mouse epidermis prompted us to identify proteins that carry the Galα1–3Gal epitope in murine epidermis. Because all the observed glycans having the Galα1–3Gal epitope were biantennary oligosaccharides, we used ConA as an affinity reagent for the enrichment of the glycopeptides of interest. Immobilized

TABLE I

Observed signals of oligosaccharides released from murine skin glycoprotiens

Oligosaccharides indicated with an asterisk were detected also by a two-dimensional (2D) mapping technique. Structures were detemined by a two-dimensional mapping technique combined with sequential exoglycosidase digestions. Green square, GlcNAc; light blue square, GalNac; yellow circle, Man; dark blue circle, Gal; red inverted triangle; Hex, hexose; HexNac, *N*-acetylhexosamine; dHex, deoxyhexose.

No.	Observed (m/z)	compositon	epidermis Relative abundance (%) mean ± S.D. (n=3)		2D structures	dermis Relative abundance (%) mean ± S.D. (n=3)		2D structures
1	1016.4424	(Hex)1 (HexNAc)2	0.1 ±	0.1		0.2 ±	0.2	
2	1178.4952	(Hex)2 (HexNAc)2	6.6 ±	1.5		1.1 ±	0.6	
3	1324.5531	(Hex)2 (HexNAc)2 (Deoxyhexose)1	2.7 ±	0.5		1.4 ±	0.6	
4	1340.548	(Hex)3 (HexNAc)2	11.2 ±	0.8		1.3 ±	0.7	
5	1381.5748	(Hex)2 (HexNAc)3	0.3 ±	0.1		0.0 ±	0.0	
6	1486.6059	(Hex)3 (HexNAc)2 (Deoxyhexose)1	5.5 ±	2.0 *		0.6 ±	0.2	
7	1502.6008	(Hex)4 (HexNAc)2	4.0 ±	0.8 *		0.9 ±	0.2 *	
8	1543.6274	(HexNAc)1 + (Man)3(GlcNAc)2	1.3 ±	0.1 *		0.4 ±	0.1	
9	1648.6587	(Hex)4 (HexNAc)2 (Deoxyhexose)1	0.3 ±	0.1		0.0 ±	0.0	
10	1664.6536	(Hex)2 + (Man)3(GlcNAc)2	17.0 ±	1.6 *		9.0 ±	1.6 *	
11	1689.6853	(HexNAc)1 (Deoxyhexose)1 + (Man)3(GlcNAc)2	0.5 ±	0.1 *		0.8 ±	0.2	
12	1705.6802	(Hex)1 (HexNAc)1 + (Man)3(GlcNAc)2	1.9 ±	0.6 *		0.7 ±	0.1 *	
13	1746.7068	(HexNAc)2 + (Man)3(GlcNAc)2	1.1 ±	0.1		0.3 ±	0.1	
14	1810.7115	(Hex)2 (Deoxyhexose)1 + (Man)3(GlcNAc)2	0.1 ±	0.1		0.0 ±	0.0	
15	1826.7064	(Hex)3 + (Man)3(GlcNAc)2	9.5 ±	1.1 *		5.0 ±	0.4 *	
16	1848.7384	(HexNAc)1 (NeuAc)1 + (Man)3(GlcNAc)2	0.2 ±	0.2		0.1 ±	0.2	
17	1851.7381	(Hex)1 (HexNAc)1 (Deoxyhexose)1 + (Man)3(GlcNAc)2	1.7 ±	0.3 *		0.9 ±	0.3 *	
18	1867.733	(Hex)2 (HexNAc)1 + (Man)3(GlcNAc)2	0.7 ±	0.1		1.1 ±	0.2 *	
19	1892.7647	(HexNAc)2 (Deoxyhexose)1 + (Man)3(GlcNAc)2	0.5 ±	0.0 *		2.0 ±	0.6 *	
20	1908.7596	(Hex)1 (HexNAc)2 + (Man)3(GlcNAc)2	1.6 ±	0.1 *		0.5 ±	0.1 *	
21	1949.7862	(HexNAc)3 + (Man)3(GlcNAc)2	0.3 ±	0.0		0.0 ±	0.0	
22	1988.7592	(Hex)4 + (Man)3(GlcNAc)2	6.1 ±	0.6 *		2.2 ±	0.1 *	
23	1994.7963	(HexNAc)1 (Deoxyhexose)1 (NeuAc)1 + (Man)3(GlcNAc)2	0.1 ±	0.1		0.0 ±	0.0	
24	2010.7912	(Hex)1 (HexNAc)1 (NeuAc)1 + (Man)3(GlcNAc)2	0.1 ±	0.2		0.3 ±	0.0	
25	2013.7909	(Hex)2 (HexNAc)1 (Deoxyhexose)1 + (Man)3(GlcNAc)2	0.6 ±	0.2		0.5 ±	0.1	
26	2026.7912	(Hex)1 (HexNAc)1 (NeuGc)1 + (Man)3(GlcNAc)2	0.1 ±	0.1		0.5 ±	0.1	
27	2029.7858	(Hex)3 (HexNAc)1 + (Man)3(GlcNAc)2	0.4 ±	0.2 *		0.9 ±	0.0 *	
28	2054.8175	(Hex)1 (HexNAc)2 (Deoxyhexose)1 + (Man)3(GlcNAc)2	0.5 ±	0.1 *		1.7 ±	0.4 *	
29	2070.8124	(Hex)2 (HexNAc)2 + (Man)3(GlcNAc)2	1.9 ±	0.5 *		5.7 ±	0.5 *	
30	2095.8441	(HexNAc)3 (Deoxyhexose)1 + (Man)3(GlcNAc)2	0.1 ±	0.1		0.6 ±	0.1 *	
31	2111.839	(Hex)1 (HexNAc)3 + (Man)3(GlcNAc)2	0.5 ±	0.1		0.2 ±	0.2	
32	2150.812	(Hex)5 + (Man)3(GlcNAc)2	6.3 ±	0.3 *		2.4 ±	0.6 *	
33	2152.8656	(HexNAc)4 + (Man)3(GlcNAc)2	0.0 ±	0.0		0.0 ±	0.0	
34	2156.8491	(Hex)1 (HexNAc)1 (Deoxyhexose)1 (NeuAc)1 + (Man)3(GlcNAc)2	0.0 ±	0.0		0.0 ±	0.0	
35	2172.844	(Hex)2 (HexNAc)1 (NeuAc)1 + (Man)3(GlcNAc)2	0.2 ±	0.1		0.6 ±	0.1	
36	2175.8437	(Hex)3 (HexNAc)1 (Deoxyhexose)1 + (Man)3(GlcNAc)2	0.2 ±	0.0		0.0 ±	0.0	
37	2188.844	(Hex)2 (HexNAc)1 (NeuGc)1 + (Man)3(GlcNAc)2	0.1 ±	0.1		0.8 ±	0.1	
38	2191.8386	(Hex)4 (HexNAc)1 + (Man)3(GlcNAc)2	0.3 ±	0.0		0.0 ±	0.0	
39	2216.8703	(Hex)2 (HexNAc)2 (Deoxyhexose)1 + (Man)3(GlcNAc)2	2.8 ±	0.3 *		14.6 ±	1.5 *	
40	2232.8652	(Hex)3 (HexNAc)2 + (Man)3(GlcNAc)2	0.4 ±	0.1		0.0 ±	0.0	
41	2257.8969	(Hex)1 (HexNAc)3 (Deoxyhexose)1 + (Man)3(GlcNAc)2	0.5 ±	0.1		0.7 ±	0.1 *	
42	2273.8918	(Hex)2 (HexNAc)3 + (Man)3(GlcNAc)2	0.3 ±	0.1		0.0 ±	0.1	
43	2298.9235	(HexNAc)4 (Deoxyhexose)1 + (Man)3(GlcNAc)2	0.5 ±	0.0		0.0 ±	0.0	
44	2312.8648	(Hex)6 + (Man)3(GlcNAc)2	4.1 ±	0.7 *		1.7 ±	0.8 *	
45	2334.8968	(Hex)3 (HexNAc)1 (NeuAc)1 + (Man)3(GlcNAc)2	0.1 ±	0.2		0.4 ±	0.0	
46	2350.8968	(Hex)3 (HexNAc)1 (NeuGc)1 + (Man)3(GlcNAc)2	0.0 ±	0.0		0.5 ±	0.0	
47	2359.9285	(Hex)1 (HexNAc)2 (Deoxyhexose)1 (NeuAc)1 + (Man)3(GlcNAc)2 (HexNAc)2 (Deoxyhexose)2 (NeuGc)1 + (Man)3(GlcNAc)2	0.0 ±	0.0		0.3 ±	0.2	

TABLE I—*continued*

No.	Observed (m/z)	compositon	epidermis Relative abundance (%) mean ± S.D. (n=3)		2D structures	dermis Relative abundance (%) mean ± S.D. (n=3)		2D structures
48	2362.9282	(Hex)2 (HexNAc)2 (Deoxyhexose)2 + (Man)3(GlcNAc)2	1.3 ±	0.2		0.2 ±	0.2	
49	2375.9234	(Hex)2 (HexNAc)2 (NeuAc)1 + (Man)3(GlcNAc)2	0.0 ±	0.0		1.1 ±	0.2	
50	2378.9231	(Hex)3 (HexNAc)2 (Deoxyhexose)1 + (Man)3(GlcNAc)2	0.7 ±	0.1 *		0.7 ±	0.1	
51	2391.9234	(Hex)2 (HexNAc)2 (NeuGc)1 + (Man)3(GlcNAc)2	0.1 ±	0.1		5.2 ±	0.4	
52	2394.918	(Hex)4 (HexNAc)2 + (Man)3(GlcNAc)2	0.7 ±	0.1 *		0.0 ±	0.0	
53	2419.9497	(Hex)2 (HexNAc)3 (Deoxyhexose)1 + (Man)3(GlcNAc)2	0.4 ±	0.0		0.5 ±	0.1	
54	2435.9446	(Hex)3 (HexNAc)3 + (Man)3(GlcNAc)2	0.3 ±	0.1 *		0.0 ±	0.0 *	
55	2476.9712	(Hex)2 (HexNAc)4 + (Man)3(GlcNAc)2	0.6 ±	0.1		0.0 ±	0.0	
56	2489.9915	(HexNAc)2 (Deoxyhexose)3 (NeuAc)1 + (Man)3(GlcNAc)2	0.0 ±	0.0		0.0 ±	0.0	
57	2505.9864	(Hex)1 (HexNAc)2 (Deoxyhexose)2 (NeuAc)1 + (Man)3(GlcNAc)2	0.0 ±	0.0		0.3 ±	0.3	
58	2508.9861	(Hex)2 (HexNAc)2 (Deoxyhexose)3 + (Man)3(GlcNAc)2	0.4 ±	0.0		0.0 ±	0.0	
59	2518.9816	(Hex)1 (HexNAc)2 (NeuAc)2 + (Man)3(GlcNAc)2	0.0 ±	0.0		0.2 ±	0.1	
60	2521.9813	(Hex)2 (HexNAc)2 (Deoxyhexose)1 (NeuAc)1 + (Man)3(GlcNAc)2	0.1 ±	0.1		1.1 ±	0.2	
61	2524.981	(Hex)3 (HexNAc)2 (Deoxyhexose)2 + (Man)3(GlcNAc)2	0.4 ±	0.0		0.0 ±	0.0	
62	2537.9813	(Hex)2 (HexNAc)2 (Deoxyhexose)1 (NeuGc)1 + (Man)3(GlcNAc)2	0.1 ±	0.1		15.3 ±	2.1	
63	2540.9759	(Hex)4 (HexNAc)2 (Deoxyhexose)1 + (Man)3(GlcNAc)2	1.2 ±	0.0 *		0.0 ±	0.0	
64	2553.9762	(Hex)3 (HexNAc)2 (NeuGc)1 + (Man)3(GlcNAc)2	0.1 ±	0.1		0.0 ±	0.0	
65	2560.0082	(HexNAc)3 (NeuAc)2 + (Man)3(GlcNAc)2	0.0 ±	0.0		0.2 ±	0.4	
66	2563.0079	(Hex)1 (HexNAc)3 (Deoxyhexose)1 (NeuAc)1 + (Man)3(GlcNAc)2	0.0 ±	0.0		0.0 ±	0.0	
67	2582.0025	(Hex)3 (HexNAc)3 (Deoxyhexose)1 + (Man)3(GlcNAc)2	0.2 ±	0.0		0.5 ±	0.5 *	
68	2681.0344	(Hex)2 (HexNAc)2 (NeuAc)2 + (Man)3(GlcNAc)2	0.0 ±	0.0		0.1 ±	0.3	
69	2684.0341	(Hex)3 (HexNAc)2 (Deoxyhexose)1 (NeuAc)1 + (Man)3(GlcNAc)2 (Hex)2 (HexNAc)2 (Deoxyhexose)2 (NeuGc)1 + (Man)3(GlcNAc)2	0.1 ±	0.1		0.4 ±	0.1	
70	2713.0344	(Hex)2 (HexNAc)2 (NeuGc)2 + (Man)3(GlcNAc)2	0.1 ±	0.1		6.1 ±	1.7	
71	2725.0607	(Hex)2 (HexNAc)3 (Deoxyhexose)1 (NeuAc)1 + (Man)3(GlcNAc)2	0.0 ±	0.0		0.0 ±	0.0	
72	2741.0556	(Hex)3 (HexNAc)3 (NeuAc)1 + (Man)3(GlcNAc)2 (Hex)2 (HexNAc)3 (Deoxyhexose)1 (NeuGc)1 + (Man)3(GlcNAc)2	0.0 ±	0.0		0.2 ±	0.3	
73	2827.0923	(Hex)2 (HexNAc)2 (Deoxyhexose)1 (NeuAc)2 + (Man)3(GlcNAc)2	0.0 ±	0.0		0.5 ±	0.5	
74	2843.0923	(Hex)2 (HexNAc)2 (Deoxyhexose)1 (NeuAc)1 (NeuGc)1+ (Man)3(GlcNAc)2	0.0 ±	0.0		0.7 ±	0.2	
75	2859.0923	(Hex)2 (HexNAc)2 (Deoxyhexose)1 (NeuGc)2 + (Man)3(GlcNAc)2	0.0 ±	0.0		4.9 ±	1.6	
76	2887.1135	(Hex)3 (HexNAc)3 (Deoxyhexose)1 (NeuAc)1 + (Man)3(GlcNAc)2	0.0 ±	0.0		0.0 ±	0.0	
77	2900.1138	(Hex)2 (HexNAc)3 (NeuAc)1 (NeuGc)1 + (Man)3(GlcNAc)2 (Hex)1 (HexNAc)3 (Deoxyhexose)1 (NeuGc)2 + (Man)3(GlcNAc)2	0.0 ±	0.0		0.1 ±	0.2	
78	2903.1084	(Hex)4 (HexNAc)3 (NeuAc)1 + (Man)3(GlcNAc)2 (Hex)3 (HexNAc)3 (Deoxyhexose)1 (NeuGc)1 + (Man)3(GlcNAc)2	0.0 ±	0.0		0.4 ±	0.6	
79	3034.1454	(Hex)2 (HexNAc)2 (NeuGc)3 + (Man)3(GlcNAc)2	0.0 ±	0.0		0.4 ±	0.4	
80	3049.1663	(Hex)3 (HexNAc)3 (Deoxyhexose)2 (NeuGc)1 + (Man)3(GlcNAc)2 (Hex)4 (HexNAc)3 (Deoxyhexose)1 (NeuAc)1 + (Man)3(GlcNAc)2	0.0 ±	0.0		0.1 ±	0.1	
81	3192.2296	(Hex)3 (HexNAc)3 (Deoxyhexose)1 (NeuAc)2 + (Man)3(GlcNAc)2	0.0 ±	0.0		0.0 ±	0.0	
82	3369.2884	(Hex)5 (HexNAc)6 + (Man)3(GlcNAc)2	0.1 ±	0.2		0.0 ±	0.0	

ConA columns bind weakly to biantennary complex-type *N*-glycans, which can be eluted with 10 mM α-methylglucoside (20). Peptides were identified by off-line LC-MALDI-TOF/TOF analysis by analyzing the glycopeptide or by analyzing the peptide following PNGase F digestion.

We identified six glycoproteins with seven *N*-glycosylation sites that carry the Galα1–3Gal epitope (supplemental Fig. 1; summarized in Table II). Although we only identified a limited number of glycoproteins, they are likely to represent the major Galα1–3Gal proteins because we identified those glycopeptides with the strongest signal intensities. Among the six glycoproteins identified as carrying Galα1–3Gal, both desmoglein 1 and desmocollin 1 are components of intercellular desmosome junctions and are involved in the interaction of plaque proteins and intermediate filaments mediating cell-cell interactions (21). Integrin β4 is a glycoprotein that associates with the α6 integrin to form the α6-β4 complex, which functions as a receptor for laminin. Integrin β4 also plays a critical structural role in the hemidesmosome of epithelial cells (22). H2-K1 and H2-D1 are components of MHC class I (MHC-I),